Tampereen teknillinen korkeakoulu
Julkaisuja 350

Tampere University of Technology
Publications 350

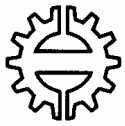

Mikko Valkama

Advanced I/Q Signal Processing for Wideband Receivers: Models and Algorithms

Tampere 2001

Tampereen teknillinen korkeakoulu
Julkaisuja 350

Tampere University of Technology
Publications 350

Mikko Valkama

Advanced I/Q Signal Processing for Wideband Receivers: Models and Algorithms

Thesis for the degree of Doctor of Technology to be presented with due permission for public examination and criticism in Auditorium HB115, Hermitec at Tampere University of Technology, on the 23rd of November 2001, at 12 o'clock noon.

Tampere 2001

ISBN 952-15-0715-2 (printed)
ISBN 952-15-1418-3 (PDF)
ISSN 0356-4940

TTKK- PAINO, Tampere 2001

Abstract

In-phase/quadrature (I/Q) signal processing is a fundamental tool in processing of bandpass signals. Especially in radio transceivers, it offers an effective solution to the inherent image signal problem without exhaustive RF image reject filtering, resulting in a clearly simplified analog front-end. This kind of approach is taken, e.g., in the so called low-IF receiver. When I/Q processing is implemented using practical analog electronics, however, the amplitudes and phases of the I and Q branches can never be perfectly matched. This compromises the theoretically infinite image signal attenuation in a dramatic manner, making it insufficient as such for most receiver architectures. Therefore, digital techniques enhancing this image attenuation play an important role in using simple analog front-ends in future high-performance highly-integrated wireless receivers.

In this thesis, novel I/Q signal processing techniques for wideband receivers are presented. The main emphasis is on the downconversion/demodulation process and the related image signal problem. The essence of the thesis concentrates on digital I/Q imbalance compensation. An analytical signal model for imbalanced analog front-end processing is derived and, based on this model, the imbalance compensation is formulated in a novel manner. The compensation problem is viewed as a signal enhancement task where two properly generated baseband observations are processed digitally. Two alternative digital techniques are proposed and analyzed. The first method stems from the well-known principle of adaptive interference cancellation whereas the second one is based on more recent blind signal separation. The compensation performance of both methods is studied analytically and using computer simulations. The results indicate that the proposed methods can provide sufficient compensation performance with reasonable assumptions. In general, since no known training signals are needed, the compensation can be performed blindly during the normal receiver operation. Furthermore, the most challenging situations of frequency-dependent and time-varying imbalances can be handled as well.

In addition to the digital enchancement of analog front-end image attenuation, bandpass sampling based digital quadrature demodulation techniques are also discussed. More specifically, a detailed analysis of the basic second-order sampling scheme is given and its connection to the ideal I/Q sampling is addressed. Due to the inherent timing offset between the I and Q branch signals, the resulting image attenuation of the second-order sampling scheme is limited and shown to be insufficient as such for multichannel signals. To improve the demodulation quality, fixed interference cancellation and fractional delay filtering based novel compensation techniques are proposed. As shown by the theoretical analysis as well as design examples, theoretical image attenuations in the order of 100 dB are easily achievable using either of the proposed approaches.

Preface

The research work presented in this thesis was carried out during the years 1999-2001 at the Telecommunications Laboratory, Tampere University of Technology, Tampere, Finland. Therefore, I want to thank all the current and earlier personnel of the Telecommunications Laboratory for providing the most inspiring and pleasant working environment.

I would like to express my deepest gratitude to Prof. Markku Renfors and Prof. Visa Koivunen, my thesis supervisors, for their invaluable guidance, continuous support, and friendship during the research work leading to this thesis. I am also grateful to Prof. Iiro Hartimo, Director of the Graduate School in Electronics, Telecommunications, and Automation (GETA), and to the thesis reviewers, Research Prof. Aarne Mämmelä and Dr. Kari Kalliojärvi.

The research work was financially supported by the graduate school GETA, the Academy of Finland, the Nokia Foundation, and the Finnish Cultural Foundation, all of which are gratefully acknowledged. I would also like to thank Tarja Erälaukko and Sari Kinnari, secretaries of our laboratory, and Marja Leppäharju, secretary of the GETA, for their help with practical matters.

Finally, I wish to express my warmest thanks to my parents Raimo and Marja-Leena Valkama and to Outi-Maaria Juutilainen for their endless love and support during this work and especially during the everyday life.

Tampere, November 2001.

Mikko Valkama

Contents

Abstract iii

Preface v

List of Publications ix

List of Supplementary Publications xi

List of Abbreviations xiii

List of Principal Symbols xv

1 Introduction 1

1.1 Motivation and Background 1

1.2 Scope of the Thesis 2

1.3 Outline and Main Results of the Thesis 5

2 I/Q Signal Processing 7

2.1 Complex Signals and Systems 7

2.2 Bandpass Transmission 8

2.3 Frequency Translations and Filtering 9

2.4 Imbalance Models for I/Q Signals 12

3 Downconversion and Image Rejection in Wireless Transceivers 15

3.1 Mixing and Image Signals 16

3.2 I/Q Processing and Imbalanced Analog Front-End 20

3.3 Earlier Work on Imbalance Compensation 24

4 Statistical Signal Processing Techniques for Imbalance Compensation 29

4.1 Two Baseband Observations 29

4.2 Interference Cancellation (IC) Based Compensation 32

4.3 Blind Source Separation (BSS) Based Compensation 34

4.4 Performance Results 36
4.5 Comparisons and Practical Matters 43
4.6 System-Level Aspects 45

5 Bandpass Sampling and Quadrature Demodulation 47
5.1 Sampling of Bandpass Signals 47
5.2 Second-Order Sampling 49

6 Digitally Enhanced Second-Order Sampling Scheme 51
6.1 Continuous-Time System Model and Image Attenuation 51
6.2 Fixed Interference Cancellation (IC) 54
6.3 Fractional Delay (FD) Filtering 56
6.4 Comparisons and Practical Considerations 59

7 Conclusions 61

8 Summary of Publications 63
8.1 Author's Contribution to the Publications 64

Bibliography 65

Publications 73

List of Publications

This thesis consists of the following publications:

[P1] M. Valkama and M. Renfors, “Advanced DSP for I/Q imbalance compensation in a low-IF receiver,” in *Proc. IEEE International Conference on Communications*, New Orleans, LA, USA, June 2000, pp. 768-772.

[P2] M. Valkama, M. Renfors, and V. Koivunen, “On the performance of interference canceller based I/Q imbalance compensation,” in *Proc. IEEE International Conference on Acoustics, Speech, and Signal Processing*, Istanbul, Turkey, June 2000, pp. 2885-2888.

[P3] M. Valkama, M. Renfors, and V. Koivunen, “Blind source separation based I/Q imbalance compensation,” in *Proc. IEEE Symposium 2000 on Adaptive Systems for Signal Processing, Communications, and Control*, Lake Louise, AL, Canada, Oct. 2000, pp. 310-314.

[P4] M. Valkama, M. Renfors, and V. Koivunen, “Advanced methods for I/Q imbalance compensation in communication receivers,” *IEEE Transactions on Signal Processing*, vol. 49, pp. 2335-2344, Oct. 2001.

[P5] M. Valkama, M. Renfors, and V. Koivunen, “Compensation of frequency-selective I/Q imbalances in wideband receivers: Models and algorithms,” in *Proc. Third IEEE Workshop on Signal Processing Advances in Wireless Communications*, Taoyuan, Taiwan, R.O.C., Mar. 2001, pp. 42-45.

[P6] M. Valkama and M. Renfors, “A novel image rejection architecture for quadrature radio receivers,” submitted to *IEEE Transactions on Circuits and Systems II*.

[P7] M. Valkama and M. Renfors, “Second-order sampling of wideband signals,” in *Proc. IEEE International Symposium on Circuits and Systems*, Sydney, Australia, May 2001, pp. 801-804.

List of Supplementary Publications

[S1] M. Valkama and M. Renfors, “Digital filter design for I/Q imbalance compensation,” in *Proc. X European Signal Processing Conference*, Tampere, Finland, Sept. 2000, pp. 1497-1500.

[S2] M. Valkama, M. Renfors, and V. Koivunen, “BSS based I/Q imbalance compensation in communication receivers in the presence of symbol timing errors,” in *Proc. Second International Workshop on Independent Component Analysis and Blind Signal Separation*, Helsinki, Finland, June 2000, pp. 393-398.

[S3] M. Valkama, “I/Q imbalance compensation on measured low-IF receiver front-end signals,” Telecommunications Laboratory, Tampere University of Technology, Tampere, Finland, Tech. Rep. 1-2001, Sept. 2001.

List of Abbreviations

AGC	automatic gain control
AMPS	Advanced Mobile Phone System
A/D	analog-to-digital
BPF	bandpass filter
BSS	blind source separation; blind signal separation
DC	direct current
DSP	digital signal processing
D/A	digital-to-analog
EASI	equivariant adaptive separation via independence
FD	fractional delay
FIR	finite impulse response
FM	frequency modulation
FT	Fourier transform
GMSK	Gaussian minimum-shift keying
GSM	Global System for Mobile Communications
HF	high frequency
HOS	higher-order statistics
HT	Hilbert transform
IC	interference cancellation
IF	intermediate frequency
IIR	infinite impulse response
IR	image rejection
I/Q	in-phase/quadrature

LMS	least-mean-square
LNA	low-noise amplifier
LO	local oscillator
LPF	lowpass filter
LS	least-squares
MBD	multichannel blind deconvolution
MSE	mean-squared error
MSK	minimum-shift keying
M-PSK	M-ary phase-shift keying
NF	noise figure
NMT	Nordic Mobile Telephone
PAM	pulse-amplitude modulation
PSK	phase-shift keying
QAM	quadrature amplitude modulation
QoS	quality of service
QPSK	quaternary phase-shift keying
RF	radio frequency
RLS	recursive least-squares
SD	steepest-descent
SIR	signal-to-interference ratio
SNR	signal-to-noise ratio
SWR	software radio
WLS	weighted least-squares
WSS	wide-sense stationary

List of Principal Symbols

$\mathbf{A}_k$	mixture coefficients
$A_I(f)$, $A_Q(f)$	general I and Q branch imbalance functions
B	bandwidth
c_k	fixed IC filter impulse response
$\mathbf{C}$	total system matrix
$C(f), C(e^{j\omega})$	fixed IC filter frequency response
$C_{\mathrm{OPT}}(f)$	optimum fixed IC filter frequency response
d	fractional delay
d_k	FD filter impulse response
$d(t)$, $d(n)$	desired signal observation
$D(f), D(e^{j\omega})$	FD filter frequency response
$D_{\mathrm{OPT}}(e^{j\omega})$	optimum digital FD filter frequency response
$\det(\cdot)$	determinant
$e_0(n)$	generalized error in LS linear model
E_{FD}	approximation error in FD filter design
E_{IC}	approximation error in fixed IC filter design
$E(\cdot)$	statistical expectation
f_C	center-frequency
f_{IF}	intermediate frequency
f_S	sampling frequency
$f(x)$, $\mathbf{f}(\mathbf{x})$	non-linear function
$F\{\cdot\}$	Fourier transform
g	amplitude imbalance coefficient

$G_1(f), G_2(f)$	general imbalance functions
$\mathbf{H}(\mathbf{x})$	adaptation function
$H_{\mathrm{D}}(f)$	frequency response of a time delay
$H_{\mathrm{HT}}(f)$	Hilbert transformer frequency response
$H_I(f), H_Q(f)$	receiver I and Q branch frequency responses
$H_{\mathrm{LPF}}(f)$	lowpass filter frequency response
$H_{\mathrm{NOM}}(f)$	nominal frequency response
i, k, n	integers
$i(t)$	baseband equivalent image signal
$\mathbf{I}$	identity matrix
$I(n), Q(n)$	in-phase and quadrature sample streams
j	imaginary unit
J_{MSE}	MSE cost function
J_{WLS}	WLS cost function
K_1, K_2	general imbalance coefficients
kurt(·)	kurtosis
$L, L(f)$	image signal attenuation
$L_{\mathrm{S}}(f)$	image attenuation of the basic second-order sampling scheme
$L_{\mathrm{S}}^{\mathrm{FD}}(f)$	image attenuation of the FD filter enhanced second-order sampling scheme
$L_{\mathrm{S}}^{\mathrm{IC}}(f)$	image attenuation of the IC filter enhanced second-order sampling scheme
M	amount of data samples in LS/WLS estimation
N	filter length parameter
P_X	power of $x(t)$
r	subsampling ratio
$r(t)$	received bandpass signal
Re[·]	real part
$\mathbf{s}(n)$	source vector
$s(t)$	baseband equivalent desired signal
SIR_{BSS}	general SIR of the BSS based compensator

$SIR_{\mathrm{BSS}}^{\mathrm{EASI}}$	SIR of the EASI BSS compensator
SIR_{IC}	general SIR of the IC based compensator
$SIR_{\mathrm{IC}}^{\mathrm{MSE}}$	SIR of the minimum MSE IC compensator
$SIR_{\mathrm{IC}}^{\mathrm{LMS}}$	SIR of the LMS IC compensator
$SIR_{\mathrm{IC}}^{\mathrm{RLS}}$	SIR of the RLS IC compensator
SIR_X	SIR of $x(t)$
T_S	sample interval
$v(t)$, $v(n)$	interference observation
w_k	IC filter impulse response
w_{LMS}	single-tap LMS IC filter coefficient
w_{MSE}	single-tap minimum MSE IC filter coefficient
w_{OPT}	single-tap optimum IC filter coefficient
w_{WLS}	single-tap WLS IC filter coefficient
$\mathbf{W}_k$	multichannel separating filter impulse response
$\mathbf{x}(n)$	observation vector
$x_{\mathrm{LO}}(t)$	local oscillator signal
$x_I(t)$, $x_Q(t)$	in-phase and quadrature components of $x(t)$
$x'(t)$	imbalanced signal
$\hat{x}(t)$	Hilbert transform of $x(t)$ or estimate of $x(t)$ [1]
$X(f)$	spectrum (Fourier transform) of $x(t)$
$\mathbf{y}(n)$	separator output vector
$z(t)$	lowpass equivalent signal of $r(t)$
α	step-size parameter (EASI algorithm)
ΔT	sampling time offset
$\Delta\Phi$	phase difference

[1] This notation is conventional for both quantities. We shall rely on context to distinguish the Hilbert transform and the estimate interpretations.

ε	difference between the minimum MSE and LMS IC filter coefficients
ϕ	phase imbalance coefficient
$\Phi_X(f)$	power density spectrum of $x(t)$
γ, κ	non-linear moments
λ	weighting factor (RLS algorithm)
μ	step-size parameter (LMS algorithm)
ω	normalized (digital) frequency

$(\cdot)^T$	transposition
$(\cdot)^H$	Hermitian transposition
$(\cdot)^*$	complex conjugation
$\lvert\cdot\rvert$	absolute value
$\lfloor\cdot\rfloor$	nearest integer less than or equal to the argument

Chapter 1

Introduction

1.1 Motivation and Background

Ever since the rather primitive yet fundamental experiments on radio transmission by Lodge and Marconi in the late 19th century [14], [23], [38], the ability to communicate with people, independently of location, time, and environment, has evolved tremendously. However, due to technical and practical problems with wireless equipment, the utilization of wireless transmission was mainly limited to broadcasting applications as well as to professional and military use for several decades. Just in the early 1980s, after the development of the cellular concept, the first major public wireless system, known as the Advanced Mobile Phone System (AMPS), was introduced in the United States. This was shortly followed by the Nordic Mobile Telephone (NMT) system in Scandinavia. Both of these systems were based on analog frequency modulation (FM) and supported only speech services.

Currently, several digital cellular systems, such as the Global System for Mobile Communications (GSM), exist in different parts of the world (see, e.g., [70] for a short review). These systems are based on digital modulation techniques and are used mainly for voice applications as well as for low rate (up to tens of kilobits per second) data transmission. Furthermore, new more sophisticated systems providing high speed (up to several Megabits per second) wireless data transmission will be deployed in the coming years. Instead of converging to a single worldwide system, it seems that various different standards will co-exist in the future. Another reason for a multitude of standards is the emergence of different wireless services and applications, requiring different data rates and different quality of service (QoS) for the radio interface [11], [34], [56]. In order to make these various systems and services accessible using a single user interface, the future wireless terminals should be able to adapt themselves to the different systems and their prevailing specifications. This aspect is in general referred to as flexibility or reconfigurability [5], [12], [39], [61].

In addition to the existence of wide variety of different standards and applications, the evolution of any wireless system is heavily influenced by practical, political, and economical matters. From the consumer point of view, in addition to the previous flexibility aspect, the wireless equipment should be small and light for better portability, as well as of low price for better affordability. As a consequence, the current research emphasis is directed on wireless technologies and configurations suitable for integration on a single silicon chip [2], [3], [21], [39], [49], [59].

In order to reach or at least approach the above-mentioned goal of a single-chip, flexible wireless device supporting multiple services and standards, the role of digital signal processing (DSP) techniques is becoming more and more important [2], [21], [26], [28], [39], [49], [59], [82]. Enabled by the recent advances in sampling and analog-to-digital (A/D) conversion technologies, the current trend, especially in the receiver side, is to move the interface between the transceiver analog and digital parts closer to the antenna [21], [39], [40], [59]. In this way, more and more of the receiver signal processing can be implemented digitally, increasing the flexibility, configurability, and integrability. Ultimately, all the transceiver functionalities, such as modulation, channel selection, and demodulation, are defined and implemented in software. In general, this kind of architectures are usually referred to as the software-defined radio or simply software radio (SWR) approach [5], [34], [39], [40], [61], [83], [94], [95]. Thus, by means of a common hardware platform, the future wireless terminals could be adaptable to any radio interface by simply changing the DSP software.

From both the flexibility and integrability point of views, the traditional superheterodyne receiver is not practical. Instead, architectures with greatly simplified and possibly wideband analog front-ends are needed [2], [20], [21], [39], [59], [71]. In this context, the I/Q signal processing techniques presented in this thesis offer novel solutions to the fundamental challenges in transceiver signal processing. Especially in the receiver side, I/Q processing offers an effective solution to the inherent image signal problem, thus relaxing the general requirements for RF filtering in a considerable manner. This, in turn, simplifies the receiver analog front-end and its implementation as a whole.

1.2 Scope of the Thesis

Independently of the applied architecture, one of the most fundamental functions of any radio receiver is to downconvert the desired channel signal from radio frequencies (RF) closer to baseband. In general, the presence of possibly much stronger other channel signals makes this

a challenging task. Especially, as will be discussed in more detail later on, attenuating the so called image band signal is one of the most crucial and challenging tasks in this context.

Traditionally, the image band signal is attenuated using a costly RF image rejection (IR) filter [3], [21], [39], [49], [59], [82]. Alternatively, in order to relax the general requirements for RF filtering, one fascinating approach is to utilize analog quadrature or I/Q downconversion. This concept is presented at a general level in Figure 1–1. One possibility is to downconvert the desired user's signal directly to baseband. This is the so called direct-conversion receiver (also known as the zero-IF or homodyne receiver) [1], [59], [71], [72]. An alternative approach is to downconvert the desired user's signal to a low but non-zero intermediate frequency (IF). This kind of a receiver is generally referred to as the low-IF receiver [20], [21], [49]. In these architectures, I/Q signal processing is in theory able to perform the needed image rejection task perfectly without any RF filtering. Clearly, this simplifies the receiver analog parts and, thus, the receiver integration. Also in wideband receivers, where a collection of frequency channels (in the extreme case, the whole service band) is downconverted as a whole, quadrature processing can basically be used in a similar manner for image rejection purposes [39], [40], [48].

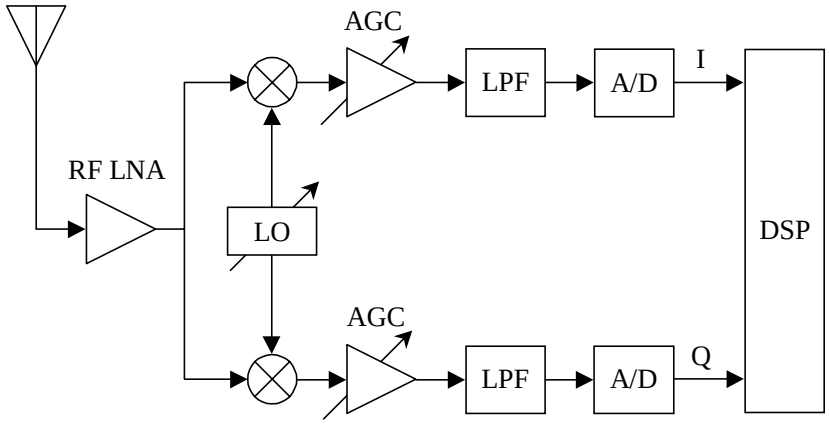

Figure 1–1: *General I/Q processing based receiver structure.*

Due to the inherent two-branch structure (I and Q), analog I/Q processing is, however, extremely vulnerable to mismatches between these two branches. In other words, since two physical signal branches and the corresponding signal processing functions need to be implemented, the relative matching of the two branches becomes vital. Now, when the I/Q processing is implemented using some practical analog circuit technologies, the two processing chains can never be exactly identical. As an example, since the I and Q branch mixers are two separate physical components, their characteristics always differ from one

another to some extent. Furthermore, the two local oscillator (LO) signals should ideally have equal amplitudes and an exact phase difference of $90°$. Again, in practice, these two signals can be realized only with a finite relative accuracy. In addition to the downconversion stage, also the amplification, filtering, and sampling functions in the I and Q branches are susceptible to relative mismatches.

In practical circuit implementations, especially in highly integrated ones, the I and Q branch amplitudes and phases can generally be matched only within 1-2% and 1-2°, respectively. In contrast to the infinite image rejection of perfectly matched I/Q processing, these levels of imbalance result only in 20-40 dB image attenuation [2], [19], [21], [39], [71], [82]. Whether this 20-40 dB image attenuation is sufficient or not, depends heavily on the applied architecture. More specifically, if the intermediate frequency is *zero*, the image band signal is the desired signal itself, and the imperfect image rejection results in a linear transformation of the original signal constellation. In this case, the above-mentioned image attenuation is adequate, at least with low-level modulations [1], [3], [71]. However, if the intermediate frequency is *non-zero*, the image band may carry a signal at the maximum allowed signal level, and the mirror[2] frequency suppression of the analog I/Q processing is far from being acceptable. Similarly in wideband receivers, the power difference of the individual channel signals can be, depending on the system specifications, as high as 50-100 dB necessitating much higher image attenuation [3], [11], [21], [39], [48], [59].

To facilitate the use of I/Q signal processing combined with simple analog front-ends, additional image attenuation must be obtained. For this purpose, analog techniques, such as the polyphase filtering discussed in [17] and [20], can be used. However, this kind of additional analog processing results in a clearly more complicated front-end circuitry, contradicting the original goal of simplifying the receiver analog parts. Digital methods, in turn, do not compomise the front-end simplicity and integrability in any way. Besides, in multichannel receivers, additional flexibility is needed in the sense that the locations of the desired channels and thus, the locations of the image channels, can vary. In general, digital compensation techniques could be a way to get around these difficulties and make simple analog front-ends feasible also in wideband receivers.

Motivated by the advances in analog-to-digital conversion technologies, bandpass sampling based digital demodulation methods, such as the second-order sampling scheme, have also started to draw some attention; see, e.g., [15], [16], [22], [25]. In the basic second-order sampling scheme, a bandpass signal is sampled in a periodically non-uniform manner

[2] The terms mirror (frequency) and image (frequency) are used interchangeably in this thesis.

and the resulting sample stream is divided into two separate data streams. This kind of digital techniques utilizing only a single analog signal branch have the natural advantage of being able to minimize the branch mismatches. However, the basic second-order sampling scheme introduces another type of mismatch, namely a small timing offset, between the two sample streams. As a result, when these two sample streams are interpreted as the sampled I and Q signals, the image attenuation capability of the basic second-order sampling technique is far from being perfect. Again, for narrowband single-channel receivers, the resulting demodulation performance may suffice but for wideband multichannel receivers, additional digital processing is needed.

1.3 Outline and Main Results of the Thesis

In this thesis, the problem of enhancing the image rejection of a practical I/Q processing based analog front-end using digital techniques is addressed in detail. Firstly, in Chapter 2, the fundamental concepts of I/Q signal processing are reviewed. Then, in Chapter 3, the various downconversion techniques are discussed with a natural emphasis on I/Q processing and image rejection in different receiver architectures. Furthermore, a linear model for an imbalanced I/Q processing based analog front-end is derived together with an explicit expression for the resulting image attenuation. This signal model forms the theoretical basis for the reminder of the thesis. A general review of the existing imbalance compensation techniques concludes Chapter 3. Motivated by the presented signal analysis, a novel idea of generating *two* baseband signals for digital imbalance compensation is proposed in Chapter 4. Relying on these observations, two alternative digital compensation methods are introduced based on statistical signal processing. Instead of trying to estimate the actual imbalance parameters, the imbalance compensation task is formulated as a blind signal estimation problem in a novel manner. A simple structure for compensation is derived based on traditional adaptive interference cancellation (IC). As an alternative, theoretically more advanced blind signal separation (BSS) techniques are also proposed for obtaining improved image rejection. Performance of the proposed solutions is analyzed in detail both analytically and through computer simulations. These analyses give formal validation to the proposed compensation techniques. Also, a comparison between the two methods regarding practical matters, such as the effects of modulation type and additive noise, is reported.

The basic approach of viewing the imbalance compensation problem as a blind signal estimation task is new in the literature of the field. The only contribution resembling our work in any sense is the one reported by Yu and Snelgrove in [93]. Though somewhat similar, the

results and techniques presented in this thesis and the ideas in [93] were discovered and developed completely independently. Furthermore, the approach in [93] is mostly heuristic lacking a clear theoretical foundation. Our results, in turn, are based on explicit signal models and build on solid theoretical problem formulation, well-motivated assumptions, and analytical performance results.

Extending further the role of digital techniques in transceiver signal processing, the second-order sampling based digital demodulation scheme is also discussed and analyzed, especially from a wideband receiver point of view. In Chapter 5, a general-level description of the various bandpass sampling based demodulation techniques is given. Then, in Chapter 6, the image rejection capability of the basic second-order sampling technique is analyzed in detail showing inferior performance if applied to multichannel receivers. In order to improve the demodulation performance, two novel digital compensation structures are introduced. One stems from the fixed interference cancellation approach whereas the other is based on fractional delay (FD) filtering techniques. Again, theoretical performances of the proposed enhanced digital demodulators are evaluated analytically. This gives a solid foundation to the design of practical compensation filters which can only approximate the derived optimum solutions. This is the most important technical contribution of this part of the thesis. In order to illustrate the effectiveness of the proposed solutions, the compensation performance is further assessed using simulation and design examples with practical filter structures and lengths.

The general conclusions of the thesis are drawn in Chapter 7. A short summary of the thesis publications [P1]-[P7] is given in Chapter 8 where the Author's contribution to the publications is clarified as well. In general, the leading idea in composing this thesis was to state the new ideas and results originally reported in [P1]-[P7] as a complete yet fluent summary. Furthermore, the selected way of presentation, especially in Chapters 2 and 5, is justified by the fact that no comprehensive treatment of I/Q signal processing and its use in various receiver architectures is available in the literature so far. Thus, in most of the forthcoming material, the signal analysis and system modelling aspects are emphasized. Much more details, especially on the performance analyses, of the proposed techniques are naturally available in the original papers [P1]-[P7].

Chapter 2

I/Q Signal Processing

In-phase/quadrature (I/Q) signal processing is a widely used tool in modulated systems and radio communications in order to take full advantage of the available resources (such as the transmission bandwidth). While most of the applications of complex-valued signals postulate digital processing, the main analog application is in frequency translations and image rejection needed in radio transmitters and receivers.

2.1 Complex Signals and Systems

In communications signal processing, it is common to use the notion of complex-valued signals. As an illustration, two oscillator signals with a 90° phase difference, $\cos(2\pi f_0 t)$ and $\sin(2\pi f_0 t)$, can be conveniently modelled as a complex oscillator $\cos(2\pi f_0 t) + j\sin(2\pi f_0 t) = e^{j2\pi f_0 t}$. In practice, a complex-valued signal is simply a pair of two real-valued signals carrying the real and imaginary parts.

The benefit of employing and processing complex-valued signals is most conveniently described in frequency domain. For a real-valued signal, say $x(t)$, the Fourier transform[3] (FT) $X(f)$ obeys the Hermitian symmetry, i.e., $X(-f) = X^*(f)$ where the superscript $(.)^*$ denotes complex conjugation [8], [26], [52], [67]. There is, however, no such symmetry for complex-valued signals in general. Therefore, by using complex arithmetic, the positive and negative frequency parts of any complex-valued signal can be processed independently. As an example, signals comprising only positive or negative frequencies, such as the complex oscillator $e^{j2\pi f_0 t}$, can be generated. In general, this kind of signals are usually referred to as analytic signals [8], [26], [33], [52], [67].

---

[3] All the signals $x(t)$ for which $\int_{-\infty}^{\infty} |x(t)|^2 \, dt < \infty$ are in general Fourier transformable. This is, however, a sufficient yet not necessary condition for the existence of a Fourier transform $X(f)$. For more details, see, e.g., [26] and [38].

2.2 Bandpass Transmission

In radio communications, the concept of complex-valued or I/Q signals was initially enabled and justified by the virtue of bandpass signal transmission. In general, using the lowpass-to-bandpass transformation, a complex-valued baseband signal $z(t) = z_I(t) + jz_Q(t)$ can be transmitted in a real-valued channel as [8], [52], [67]

$$r(t) = 2\,\mathrm{Re}[z(t)e^{j2\pi f_C t}] = 2z_I(t)\cos(2\pi f_C t) - 2z_Q(t)\sin(2\pi f_C t) \tag{2–1}$$

where f_C denotes the formal center-frequency of $r(t)$ and $\mathrm{Re}[x]$ refers to the real part of a complex-valued quantity x. Clearly, according to (2–1), *two* real-valued messages $z_I(t)$ and $z_Q(t)$ can be transmitted over the same bandwidth resulting in increased spectral efficiency. In the frequency domain, for a general complex-valued signal $z(t)$, this implies that the spectrum of $r(t)$, though Hermitian symmetric about the zero frequency, has no particular symmetry about the center-frequency f_C [26], [52], [67]. This is illustrated graphically in Figure 2–1.

Considering the recovery of the two messages $z_I(t)$ and $z_Q(t)$ (or equivalently, the complex-valued message $z(t)$) from the bandpass signal $r(t)$, a bandpass-to-lowpass transformation is needed. Again, the frequency domain interpretation is useful. Apparently, as illustrated in Figure 2–1, the spectral components around $+f_C$ and $-f_C$ are simply mirror images of each other, both containing all the information about $z(t)$. To state this in a more formal manner, the result of (2–1) can be rewritten as

$$r(t) = 2\,\mathrm{Re}[z(t)e^{j2\pi f_C t}] = z(t)e^{j2\pi f_C t} + z^*(t)e^{-j2\pi f_C t}. \tag{2–2}$$

Thus, for information recovery, either of the above spectral components can be selected for further processing by rejecting the corresponding mirror component. Notice that the actual frequency domain representation depends on whether the signals under consideration are deterministic or random. In the deterministic case, the spectrum (FT) of $r(t)$ can be written as

$$R(f) = Z(f - f_C) + Z^*(-f - f_C) \tag{2–3}$$

where $Z(f)$ denotes the FT of $z(t)$. In the wide-sense stationary (WSS) random signal case, on the other hand, the proper frequency domain representation is given in terms of the *power spectrum* as

$$\Phi_R(f) = \Phi_Z(f - f_C) + \Phi_Z(-f - f_C) \tag{2–4}$$

where $\Phi_Z(f)$ denotes the power spectrum of $z(t)$ [38], [52], [67]. Formally, from the system analysis point of view, these two expressions behave in a similar manner (complex conjugation is not needed in (2–4) since $\Phi_Z(f)$ is always real-valued). Thus, in most of the forthcoming material, the deterministic approach is taken for simplicity.

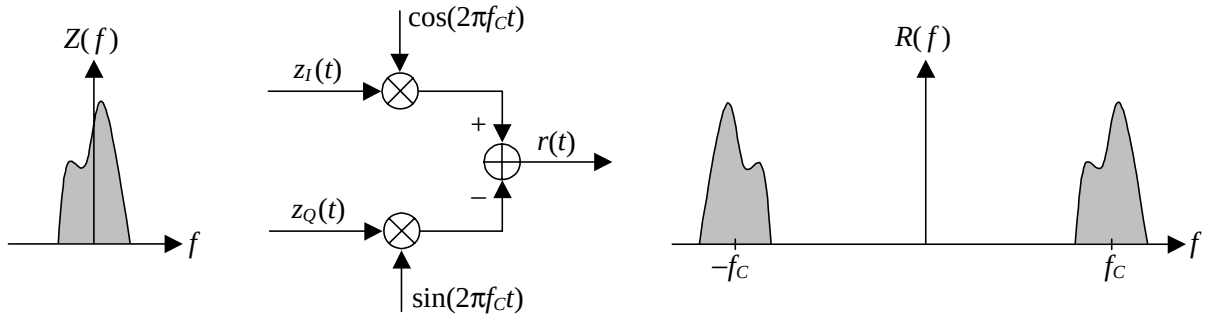

Figure 2–1: *Bandpass signal transmission.*

2.3 Frequency Translations and Filtering

As stated in Section 2.1, complex processing allows one to consider negative and positive frequencies separately. For bandpass signals, in order to select the positive frequency component, the most commonly used approach is to simply shift the spectrum of the signal by multiplying it with a complex exponential $e^{-j2\pi f_C t}$. This indeed will cause a pure frequency translation, resulting in an I/Q signal pair for which the positive and negative frequency parts of $r(t)$ are shifted around the origin and $-2f_C$, respectively. This procedure is depicted graphically in Figure 2–2 (a). Finally, the induced high frequency component around $-2f_C$ can be attenuated by applying lowpass filtering (LPF) on the I and Q signals. This concept is generally known as the quadrature or I/Q downconversion approach. Notice that in this case, the key element to the ideal separability of the original negative and positive frequency spectral components is really the 90° phase shift between the oscillator I and Q signals $\cos(2\pi f_C t)$ and $-\sin(2\pi f_C t)$.

Another alternative to attenuate the negative frequency component of (2–2) is based on a Hilbert transformer (HT) [8], [26], [33], [52], [67]. Ideally, the frequency response $H_{\mathrm{HT}}(f)$ of this kind of a filter is given by

$$H_{\mathrm{HT}}(f) = -j\,\mathrm{sgn}(f) = \begin{cases} -j & \text{for } f > 0 \\ 0 & \text{for } f = 0 \\ +j & \text{for } f < 0. \end{cases} \tag{2–5}$$

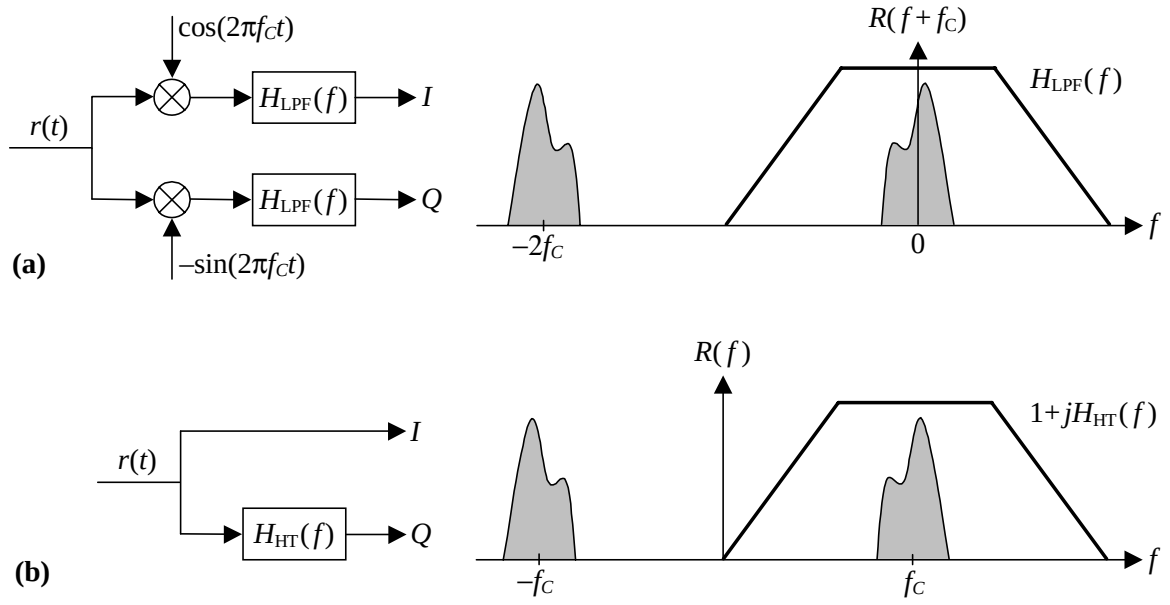

Figure 2–2: *Extraction of the positive frequency component of a bandpass signal r(t) using (a) complex exponential oscillator signal and two lowpass filters, (b) the Hilbert filter (band splitter) approach. In both cases, the key element is the* 90° *phase shift between the I and Q branch signals.*

Thus, a Hilbert filter is simply an allpass filter (except at zero frequency) that only shifts the phase of positive frequency components by $-90°$ and negative frequency components by $+90°$. In general, the terms Hilbert transformer and Hilbert filter are used interchangeably in this thesis.

In order to see how a Hilbert transformer can be used for our purposes, let the filter of (2–5) be excited by $r(t)$, producing an output signal denoted by $\hat{r}(t)$. Based on (2–2) and (2–5), the resulting signal can be expressed as

$$\begin{aligned}\hat{r}(t) &= -jz(t)e^{j2\pi f_C t} + jz^*(t)e^{-j2\pi f_C t} \\ &= 2z_I(t)\sin(2\pi f_C t) + 2z_Q(t)\cos(2\pi f_C t).\end{aligned} \tag{2–6}$$

Then, the Fourier transform of a complex signal $r(t) + j\hat{r}(t)$ is given by $[1 + jH_{\mathrm{HT}}(f)]R(f)$, where

$$1 + jH_{\mathrm{HT}}(f) = 1 + j\cdot(-j\,\mathrm{sgn}(f)) = \begin{cases} 2 & \text{for } f > 0 \\ 1 & \text{for } f = 0 \\ 0 & \text{for } f < 0. \end{cases} \tag{2–7}$$

In other words, the signal $r(t) + j\hat{r}(t)$ consists of only the positive frequency components of $r(t)$[4]. This idea is demonstrated graphically in Figure 2–2 (b). Then, to perform the desired bandpass-to-lowpass transformation, the resulting analytic signal $r(t) + j\hat{r}(t)$ can be multiplied by $\cos(2\pi f_C t)$ and lowpass filtered. Alternatively, $r(t) + j\hat{r}(t)$ can simply be multiplied by $e^{-j2\pi f_C t}$.

In practical signal processing, the true Hilbert filter is not realizable. Especially in analog signal processing, even its approximation is in general a difficult task. Luckily, in case of bandpass signals, the ideal Hilbert response of (2–5) needs to be approximated only within the signal passband, relaxing the design specifications. Occasionally, this kind of approximative Hilbert filters are also referred to as band splitters or phase splitters [20], [21], [26], [33].

To extend the discussion on Hilbert filtering and its applicability on receiver signal processing, the general spectral decomposition of a bandpass signal $r(t)$ is presented in Figure 2–3. First, for analysis purposes, define an analytic signal $x(t) = r(t) + jk\hat{r}(t)$ where the integer $k = \pm 1$. Then, the spectrum of $y(t) = x_I(t) - \hat{x}_Q(t)$ is given by $Y(f) = R(f) - kH_{\text{HT}}(f)H_{\text{HT}}(f)R(f) = [1 - kH_{\text{HT}}(f)H_{\text{HT}}(f)]R(f)$, where

$$1 - kH_{\text{HT}}(f)H_{\text{HT}}(f) = 1 - j^2 k = \begin{cases} 2 & \text{for } k = +1 \\ 0 & \text{for } k = -1 \end{cases} \tag{2–8}$$

for all frequencies $f \neq 0$. Thus, depending on the sign of k, the front-end processing (the first Hilbert transformer and the multiplier) selects either the negative or positive frequency content of the original input signal $r(t)$. After that, the subsequent processing (the second Hilbert transformer and the addition) will replace all the negative frequency components of $x(t)$ by the corresponding mirror components, thus forming again a single real-valued signal $y(t)$. This is depicted in Figure 2–3.

In the previous discussion, we applied the Hilbert filter to a real-valued bandpass signal $r(t)$. However, the main results hold for any kind of signal. Firstly, the result implied by (2–7) is directly applicable to a general complex-valued signal $x(t) = x_I(t) + jx_Q(t)$, in a sense that all the signal energy at negative and positive frequencies, respectively, can be rejected as $x(t) + j\hat{x}(t)$ and $x(t) - j\hat{x}(t)$. Furthermore, the above-mentioned spectral decomposition can be extended to any complex-valued signal $x(t)$ regardless whether it is analytic or not. To see this, the signal $x_I(t) \pm \hat{x}_Q(t)$ can simply be rewritten as $\text{Re}[x(t) \mp j\hat{x}(t)]$ for which the original

---

[4] Alternatively, if so wanted, the Hilbert concept can be used to attenuate the *positive* frequencies while preserving the *negative* ones simply as $r(t) - j\hat{r}(t)$.

signal components of $x(t)$ at either negative or positive frequencies will be replaced by the corresponding mirror components. As an example, consider the case where the complex-valued signal $x(t)$ contains a desired signal component around $+f_C$ and an undesired image signal component around $-f_C$. Now, a real-valued signal $y(t)$ with the interfering signal totally attenuated can be obtained simply as $y(t) = x_I(t) - \hat{x}_Q(t)$. This concept will be further explored in Chapter 3.

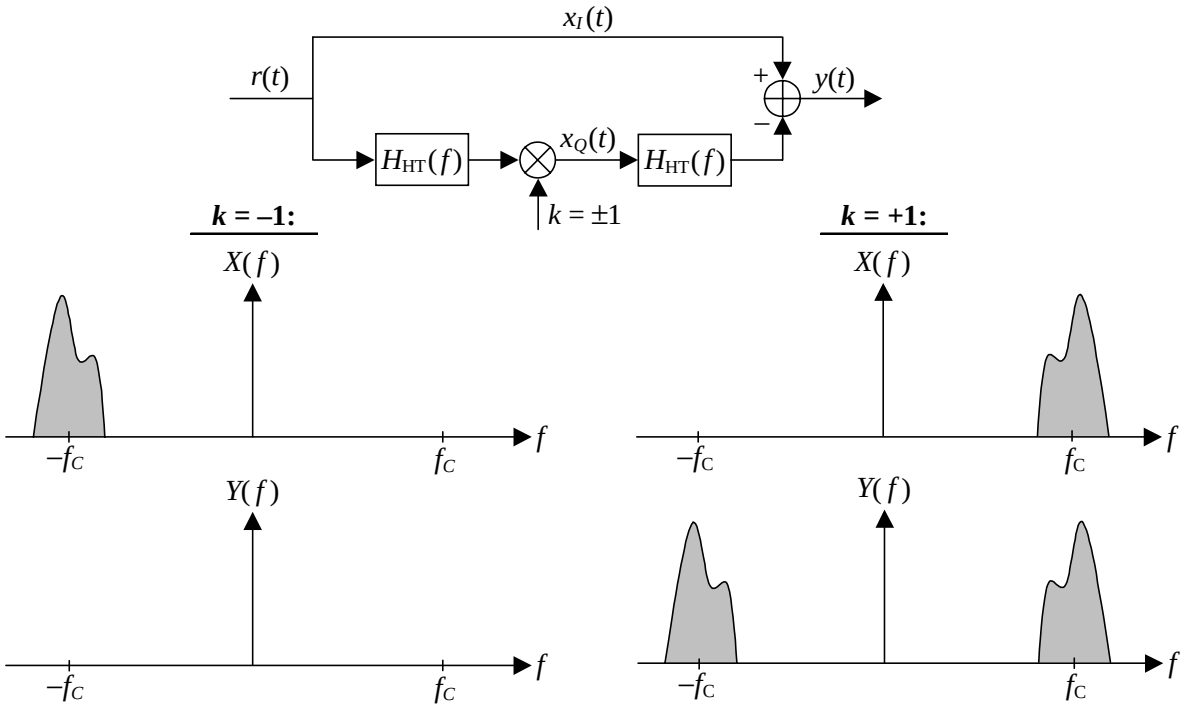

Figure 2–3: *Spectral decomposition of a bandpass signal r(t).*

2.4 Imbalance Models for I/Q Signals

The previous discussion on I/Q signal processing and its ability to process the negative and positive frequencies separately is strictly valid only if the I and Q branches are perfectly matched. Considering any practical analog circuitry, some unintentional variations between the amplitudes and phases of such a two-branch structure will always take place [3], [20], [21], [49], [59], [71], [72], [77]. Therefore, for analysis purposes, analytical models are needed to describe the imbalance effects. How these imbalances actually affect a receiver operation and especially its image attenuation capabilities is examined in detail in Chapter 3.

Narrowband Imbalance Model

To expose the fundamental effect of amplitude and phase mismatches on I/Q signals, a single positive frequency signal $z(t) = e^{j2\pi f_0 t} = \cos(2\pi f_0 t) + j\sin(2\pi f_0 t)$ is first examined. By

denoting the relative I and Q branch amplitudes by g_1 and g_2 and phases by ϕ_1 and ϕ_2, the imbalanced signal $z'(t)$ can be expressed as $z'(t) = g_1\cos(2\pi f_0 t + \phi_1) + jg_2\sin(2\pi f_0 t + \phi_2)$. Now, from the mismatch point of view, the signal $z'(t)$ can be written in a more convenient form as $z'(t) = g_1[\cos(2\pi f_0 t + \phi_1) + j(g_2/g_1)\sin(2\pi f_0 t + \phi_1 + \phi_2 - \phi_1)]$. Consequently, only the relative amplitude ratio g_2/g_1 and phase difference $\phi_2 - \phi_1$ need to be considered. Thus, to simplify the notations, we assume that $g_1 = 1$, $g_2 = g$, $\phi_1 = 0$, and $\phi_2 = \phi$, and write the imbalanced signal $z'(t)$ simply as

$$z'(t) = \cos(2\pi f_0 t) + jg\sin(2\pi f_0 t + \phi). \tag{2–9}$$

To catch the essence of the mismatch effects, the signal of (2–9) needs to be expressed in a more informative form. In effect, by simply utilizing the well-known Euler's theorem[5] for the cosine and sine terms, $z'(t)$ can be written after some manipulations as

$$\begin{aligned} z'(t) &= \left(\frac{1+ge^{j\phi}}{2}\right)e^{j2\pi f_0 t} + \left(\frac{1-ge^{-j\phi}}{2}\right)e^{-j2\pi f_0 t} \\ &= M_1 e^{j2\pi f_0 t} + M_2 e^{-j2\pi f_0 t} \end{aligned} \tag{2–10}$$

where $M_1 = (1+ge^{j\phi})/2$ and $M_2 = (1-ge^{-j\phi})/2$. Interestingly, when interpreted in the frequency domain, the result of (2–10) shows how the original complex exponential is split into two mirror frequency components with different relative complex-valued strengths M_1 and M_2. Thus, in general, the amplitude and phase mismatches cause part of the signal energy around $+f_0$ to "alias" to its mirror frequency $-f_0$, compromising the separability of the negative and positive frequency bands. The ratio between the squared amplitudes of the original component and the introduced mirror component is given by

$$L = \frac{|M_1|^2}{|M_2|^2} = \frac{1+g^2+2g\cos(\phi)}{1+g^2-2g\cos(\phi)}. \tag{2–11}$$

This represents the relative power rejection of the mirror component.

---

[5] According to the Euler's theorem, $\cos(x)$ and $\sin(x)$ can be expressed using complex-valued exponentials as $\cos(x) = \frac{e^{jx}+e^{-jx}}{2}$ and $\sin(x) = \frac{e^{jx}-e^{-jx}}{2j}$.

Wideband Imbalance Model

Considering a general complex-valued signal $z(t) = z_I(t) + jz_Q(t)$ (where $z_I(t)$ and $z_Q(t)$ are real-valued) and its complex conjugate $z^*(t) = z_I(t) - jz_Q(t)$, the corresponding Fourier transforms are given by

$$F\{z(t)\} = Z(f) = Z_I(f) + jZ_Q(f)$$

and

$$F\{z^*(t)\} = Z^*(-f) = Z_I^*(-f) - jZ_Q^*(-f) = Z_I(f) - jZ_Q(f).$$

Then, assuming that the frequency-dependent imbalance functions of the I and Q branches are represented by $A_I(f)$ and $A_Q(f)$, the Fourier transform of an imbalanced signal $z'(t)$ is here defined as

$$Z'(f) = A_I(f)Z_I(f) + jA_Q(f)Z_Q(f). \tag{2–12}$$

Even though $z_I(t)$ and $z_Q(t)$ are real-valued with Hermitian symmetric Fourier transforms, no such restriction needs to be attached to the imbalance functions $A_I(f)$ and $A_Q(f)$ in general. The expression of (2–12) can be rewritten in a more informative form as

$$Z'(f) = \left(\frac{A_I(f) + A_Q(f)}{2}\right)Z(f) + \left(\frac{A_I(f) - A_Q(f)}{2}\right)Z^*(-f) \tag{2–13}$$

which can easily be verified by a direct substitution. Based on (2–13), the mismatched signal $z'(t)$ consists of a signal component relative to $z^*(t)$ in addition to the original component $z(t)$. As in (2–10), part of the signal energy originally located at some frequency band $f_1 \ldots f_2$ will be reflected to the mirror band $-f_1 \ldots -f_2$. In general, this is the fundamental effect of time domain complex conjugation as viewed in frequency domain. Thus, (2–13) represents a generalization of the narrowband model (2–10). Notice again that only the difference between the branch imbalance functions $A_I(f)$ and $A_Q(f)$ contribute to the relative strength of the mirror component $z^*(t)$ (i.e., $Z^*(-f)$). Furthermore, a frequency-dependent image power rejection ratio could be defined in a similar manner as in (2–11). Graphical illustrations of this basic imbalance effect will be given in Chapter 3.

Chapter 3

Downconversion and Image Rejection in Wireless Transceivers

Due to the shared use of the transmission medium, the received signal consists not only of the modulated desired signal but also of many other signals. In effect, the wireless environment enables a number of different user signals to co-exist by imposing them to share different parts (frequency channels) of the radio spectrum. This is illustrated in Figure 3–1 (a). Furthermore, since the different channel signals are likely to originate from physically different sources, some of them can be very strong compared to others. Thus, in addition to amplification to compensate for the unavoidable transmission losses, the key issues in any wireless receiver are at least (*i*) tuning to select any of the received signals and (*ii*) filtering to separate the selected channel out of the possibly much more powerful adjacent channel signals. Especially, rejecting the so called image channel signal is one of the most fundamental tasks in this context [3], [21], [59], [73].

The following presentation concentrates on the most common downconversion and image rejection techniques in various wireless transceiver architectures. Naturally, the main emphasis is on the I/Q processing based image rejection techniques. Particular attention is paid to reveal and characterize the detrimental effect of the I and Q channel mismatches on the available image attenuation. Also other non-idealities of the analog front-end components, such as the non-linear distortions, are of great concern in practice. These are, however, out of the general scope of this thesis. Thus, in the analysis, a linear front-end operation is assumed. In this manner, the signal analysis can be kept at a general level being still mathematically tractable. Notice, however, that the analog front-end non-linearities are likely to affect the operation of the proposed systems to some extent in practice. Thus, these effects can and should be analyzed for each specific application (type of modulation, type of non-linearity, etc.) separately.

3.1 Mixing and Image Signals

Theoretically, the desired channel could be selected from the antenna signal directly using a tunable bandpass filter. However, since the current radio frequencies (RF) are typically on the GHz range, this is not feasible in practice. Thus, the received signal is usually translated to an intermediate frequency (IF) where the channel selection filtering can be implemented in a more feasible manner [3], [21], [59], [73].

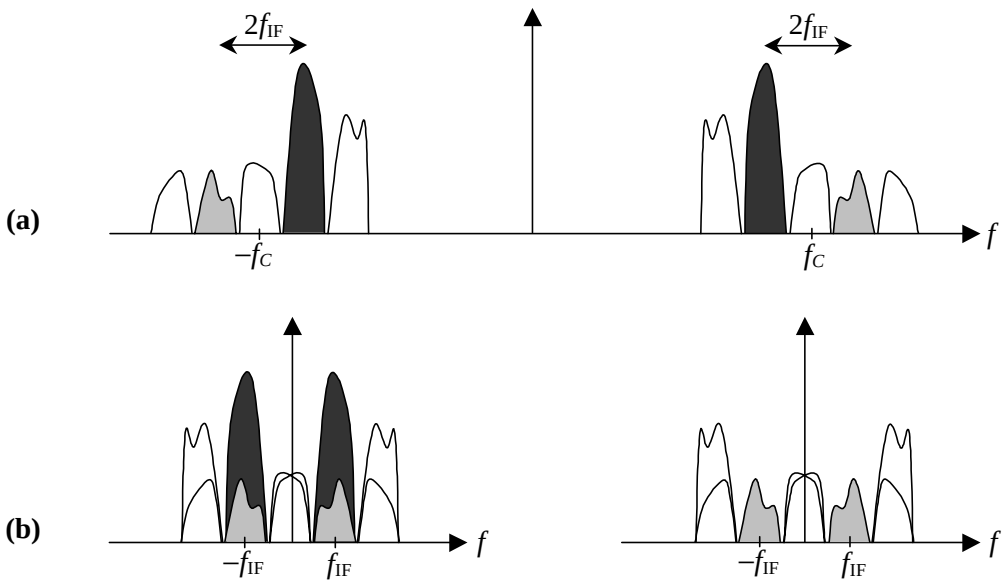

Figure 3–1: *(a) A frequency domain illustration of the received signal. A specific channel signal (grey) and its image signal (dark) are separated by* $2f_{IF}$ *and are illustrated in different colours. (b) The spectrum of the downconverted signal after real mixing and lowpass filtering without (left) and with (right) image rejection filtering.*

Real Mixing

In order to downconvert a collection of frequency channels, including the desired one, to lower frequencies, the received RF signal $r(t)$ can be mixed or multiplied with a real-valued oscillator signal, say $\cos(2\pi f_C t)$, and lowpass filtered [8], [14], [21], [38], [59]. Denoting the intermediate frequency by f_{IF}, this operation will indeed translate the signal centered at $f_C + f_{IF}$ to IF. However, since real mixing is used, also another frequency translation will take place and the signal at $f_C - f_{IF}$ will be downconverted to the intermediate frequency as well. Thus, the observable signal at IF will consist of both the desired signal and its image signal on top of each other. This phenomenon is generally referred to as the image signal problem and is depicted graphically in Figure 3–1 (b). Notice that depending on whether the

local oscillator frequency is below (low side injection) or above (high side injection) the desired channel center-frequency, also the image channel is located either below or above the desired channel. Either way, the frequency separation of any specific channel and its image channel is always $2f_{\mathrm{IF}}$. Without any loss of generality, a low side injection as depicted in Figure 3–1 is assumed throughout the rest of this thesis. The use of a high side injection would simply invert the roles of the image and desired signals in the forthcoming material.

The traditional solution to the above-mentioned image signal problem is to use some kind of image rejection (IR) filtering. In other words, the image band signal is attenuated using some kind of bandstop[6] filtering *before* the frequency translation. This, in turn, postulates a proper compromise in selecting/specifying the intermediate frequency. On one hand, a high enough intermediate frequency should be used since the desired and image signal are separated by only $2f_{\mathrm{IF}}$ and the IR filtering is performed at RF. On the other hand, a low enough intermediate frequency is needed in order to make the implementation of a highly selective channel selection filter at IF more feasible.

The previously described approach has been successfully used in traditional receiver architectures such as the superheterodyne receiver [2], [3], [8], [21], [49]. An RF image rejection filter together with a tunable local oscillator are used to attenuate the image band signal and translate the desired channel signal to IF. Tunability in the LO facilitates the use of a fixed intermediate frequency, thus enabling efficient implementation of the IF channel selection filter. However, due to the high number of discrete components and high power consumption, the superheterodyne architecture is not suitable for highly integrated implementations. Thus, architectures with more simplified analog front-ends are needed.

Complex or I/Q Mixing

A more detailed examination of Figure 3–1 leads to an important observation that only the signal components at negative (or alternatively, at positive) frequencies are actually destructive during the downconversion process [20], [21]. Thus, if one could separate the positive frequency components out of the negative ones, the image problem would be circumvented in the initial downconversion. Luckily, this can indeed be achieved using I/Q signal processing as presented in Chapter 2.

---

[6] To minimize the detrimental effects of analog front-end non-linearities, etc., the bandwidth of the signal is usually kept as low as possible. Thus, a proper bandpass filter is usually used instead of a bandstop filter in practice.

To be more precise, instead of the traditional real mixing which results in two frequency translations, complex or I/Q mixing can be used, independently of the actual desired signal modulation method [8], [14], [21], [38], [59]. Ideally, this will result in a single frequency shift eliminating the image signal problem during the downconversion. The induced high frequency term can be attenuated by lowpass filtering the I and Q branch signals as presented in Figure 2–2 (a). The spectrum of the resulting complex-valued signal is illustrated in Figure 3–2. Clearly, since the desired and image signals are perfectly separated as being located at positive and negative IFs, respectively, all the information needed to recover the signal of interest is available. In general, this kind of an approach is usually known as quadrature or I/Q downconversion.

In order to finally select the desired signal out of the adjacent channels, the IF signal is further I/Q downconverted to shift the desired signal to baseband and lowpass filtered. Since the mixer input signal is already complex-valued, a full complex-valued multiplication (4 real multiplications and 2 real additions) needs to be implemented. Alternatively, the full complex processing may be avoided in the final downconversion by first attenuating the undesired image signal components at negative frequencies using a Hilbert transformer as presented in Chapter 2. Furthermore, by considering only the real part of the resulting analytic signal, the original negative frequency components will be replaced by their mirror components. This is illustrated in Figure 3–2 (b). Thus, in practice, only the real part needs to be actually calculated and the following mixing stage will be simplified. This approach is generally known as the Hartley's image rejection concept [3], [71], [72].

Ideally, the infinite image attenuation provided by the I/Q downconversion eliminates the need for RF image reject filtering, thus relaxing the overall requirements for analog RF filtering. This clearly simplifies the analog front-end making the receiver integration more feasible. However, the perfect image attenuation is totally capitalized only if the I and Q branches are perfectly matched. This cannot be achieved using practical analog electronics and some amplitude and phase imbalance will always exist. This compromises the theoretical infinite image rejection. The fundamental effect of I/Q mismatches on the image band attenuation will be characterized analytically in Section 3.2. More specifically, a closed-form expression for the practical analog front-end image attenuation will be derived as a function of the branch imbalances.

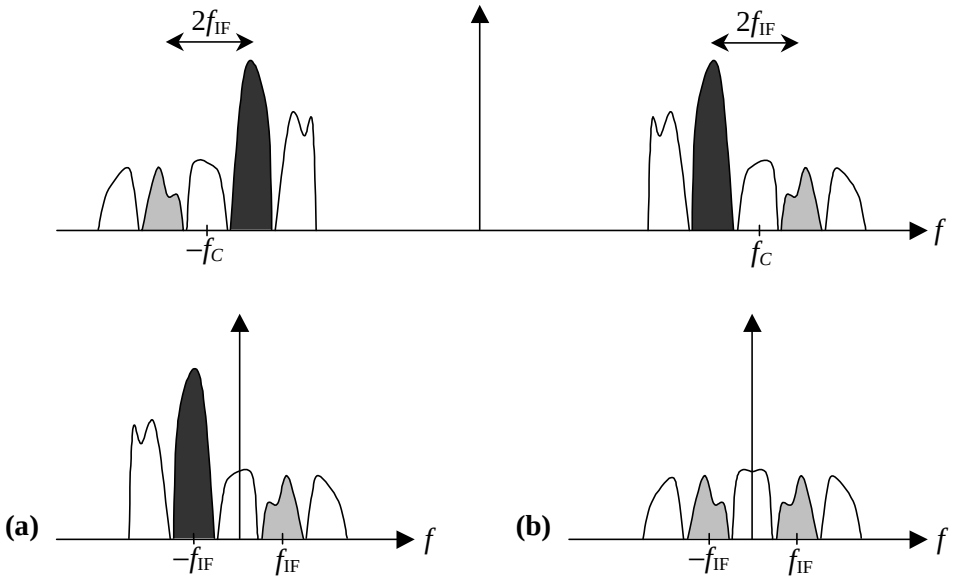

Figure 3–2: *(a) The spectrum of the received signal after quadrature downconversion and lowpass filtering. Ideally, the desired (grey) and image (dark) signals are totally separated. (b) The spectrum of the signal in part (a) after additional processing where the Hilbert transformed Q branch signal is subtracted from the I branch signal. All the signal energy at negative frequencies is replaced by the corresponding mirror components. In both cases, ideal matching of the I and Q branches is assumed.*

Whether the image rejection of imbalanced analog I/Q processing is sufficient or not, depends greatly on the applied architecture. For example, the well-known direct-conversion architecture [1], [2], [3], [59], [71], [72] as well as more recent low-IF architecture [17], [19], [20], [21], [59] both use the previous strategy of quadrature downconversion but differ fundamentally in their image rejection requirements. In the direct-conversion receiver (also known as the zero-IF or homodyne receiver), the local oscillator frequency equals the desired channel center-frequency, i.e., the desired channel signal is downconverted directly to baseband. In this case, since the IF is effectively zero, the image signal is actually the desired signal itself at negative center-frequency and the effect of imperfect self-image rejection is seen as a linear distortion of the original signal constellation. As a result, the image attenuation requirements are not very strict, especially if low-level modulations are used. In effect, the 20-40 dB image attenuation of the practical analog front-end is likely to be enough in most cases. Even though the use of zero intermediate frequency alleviates the image signal problem, the direct-conversion receiver suffers from other imperfections including the inherent LO leakage and DC-offset problems [1]-[3], [12], [59], [71]. The basic difficulty is that the LO signal leaks into the mixer RF port and self-mixes itself down to zero frequency. This self-mixing product appears directly on top of the desired signal at baseband distorting

the observable signal, especially if the desired signal has significant power/energy at low frequencies. This fundamental difficulty has strongly limited its use so far.

In the low-IF receiver, in order to reduce the effects of LO leakage and DC-offsets, the desired signal is downconverted in quadrature to a low but non-zero IF. Intermediate frequencies in the order of one or two channel bandwidths have been proposed [19], [20], [21], [49]. However, since the image signal comes now from another channel/band with a possibly very high power level, the use of a non-zero IF reintroduces the image signal problem to its fullest extent. In a "per-channel" downconverting low-IF receiver, the image signal originates from one of the nearby or adjacent channels. Though the image problem is in this case partly alleviated by the system specifications, which usually limit the power difference of the nearby channels to 10-25 dB, the 20-40 dB attenuation provided by the front-end is inadequate for most applications. In a multichannel scenario, where several channels are downconverted as a whole, the image frequency band may carry a signal at the maximum allowed signal level. Thus, for some of the channels, the image band signal can be up to 50-100 dB stronger than the desired signal, and the imbalanced analog front-end image attenuation is clearly insufficient.

Based on the previous discussion, the I/Q imbalance is in general a major concern in receivers using non-zero IF. In order to emphasize both the flexibility and integrability points of view, the forthcoming material concentrates on the general wideband scenario where a collection of frequency channels is quadrature downconverted to lower frequencies. After lowpass filtering, this multichannel signal is analog-to-digital converted and all the subsequent signal processing functions are performed using digital signal processing. This general-level formulation includes, e.g., the single-channel low-IF and direct-conversion architectures as special cases where only the signal of an isolated frequency channel needs to be detected. More generally, this approach facilitates also a flexible multichannel receiver trying the detect any of or all the signals on a collection of frequency channels (or ultimately the whole service band).

3.2 I/Q Processing and Imbalanced Analog Front-End

In our formulation, the task of analog front-end processing is to perform a multichannel bandpass-to-lowpass transformation of the received signal $r(t)$. During this process, all the analog components, such as the mixers, LO signals, branch lowpass filters, and A/D converters, affecting the I and Q branch signals contribute to the effective amplitude and

phase mismatches. Thus, to formally analyze the detrimental effect of these I/Q mismatches, proper modelling of the front-end is essential.

Front-End Model

For analysis purposes, the center-frequency of the whole received signal is here denoted by f_C. To carry out the quadrature (I/Q) downconversion, two local oscillator signals and two physical mixers are needed. Ideally, the mixers should be identical and the LO signals should have equal amplitudes and a phase difference of $90°$. Now, the mismatch effects of this quadrature downconversion stage can be modelled using an imbalanced complex-valued local oscillator signal $x_{\mathrm{LO}}(t)$ as

$$\begin{aligned} x_{\mathrm{LO}}(t) &= \cos(2\pi f_C t) - jg\sin(2\pi f_C t + \phi) \\ &= K_1 e^{-j2\pi f_C t} + K_2 e^{j2\pi f_C t} \end{aligned} \tag{3–1}$$

where the imbalance coefficients K_1 and K_2 are given by

$$\begin{aligned} K_1 &= [1 + ge^{-j\phi}]/2 \\ K_2 &= [1 - ge^{j\phi}]/2. \end{aligned} \tag{3–2}$$

In (3–1) and (3–2), g and ϕ represent the relative amplitude and phase mismatches, respectively, of both the I and Q branch LO signals and mixers. In the ideal case with perfect matching, $g = 1$ and $\phi = 0$.

After the quadrature downconversion stage, the I and Q branch signals are filtered, amplified, and sampled. Again, two physical signal branches are needed whose frequency responses can never be exactly identical in practice. The combined effect of the branch lowpass filters, amplifiers, and A/D converters can simply be modelled as a pair of two imbalanced LPF frequency responses as

$$\begin{aligned} H_{\mathrm{LPF},I}(f) &= H_{\mathrm{NOM}}(f)H_I(f) \\ H_{\mathrm{LPF},Q}(f) &= H_{\mathrm{NOM}}(f)H_Q(f). \end{aligned} \tag{3–3}$$

In (3–3), $H_{\mathrm{NOM}}(f)$ represents the nominal LPF response rejecting the high frequency components and the actual mismatch properties are characterized by $H_I(f)$ and $H_Q(f)$. Again, with perfect matching, $H_I(f) = H_Q(f)$. The complete model for the imbalanced analog front-end processing is presented in Figure 3–3.

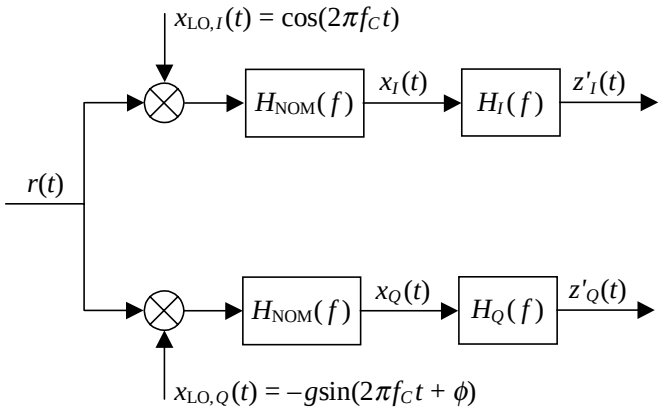

Figure 3–3: *Imbalance model for the analog front-end processing.*

Wideband Signal Model

To obtain an explicit characterization of the previously described imbalance effects on the individual channel signals, the received multichannel signal $r(t)$ can be first written as

$$r(t) = 2\,\mathrm{Re}[z(t)e^{j2\pi f_C t}] = z(t)e^{j2\pi f_C t} + z^*(t)e^{-j2\pi f_C t}\,. \tag{3–4}$$

Formally, the above expression is similar to the definition of (2–2). Here, however, $z(t)$ denotes the wideband baseband equivalent signal of the complete band of interest, consisting of multiple frequency channels. Then, in the receiver side, the received signal is multiplied by the imbalanced LO signal $x_{\mathrm{LO}}(t)$ of (3–1). Due to finite matching in the downconversion stage, *two* frequency translations instead of one desired will take place as suggested by the latter version of (3–1). Assuming that the nominal lowpass filter response rejects the resulting high frequency components, the downconverted signal $x(t) = x_I(t) + jx_Q(t)$ can be written simply as

$$x(t) = K_1 z(t) + K_2 z^*(t)\,. \tag{3–5}$$

As can be observed, since $K_2 \neq 0$, the imbalanced quadrature downconverter can suppress the image component $z^*(t)$ only by a finite amount.

Next, to analyze the effect of branch component mismatches, the signal of (3–5) can be written in terms of its I and Q components as

$$\begin{aligned} x_I(t) &= z_I(t) \\ x_Q(t) &= g\cos(\phi)z_Q(t) - g\sin(\phi)z_I(t). \end{aligned} \tag{3–6}$$

Then, the signal $z'(t) = z'_I(t) + jz'_Q(t)$ after the branch components can be expressed in frequency domain as

$$\begin{aligned} Z'(f) &= Z'_I(f) + jZ'_Q(f) \\ &= H_I(f)X_I(f) + jH_Q(f)X_Q(f) \\ &= H_I(f)Z_I(f) + jH_Q(f)[g\cos(\phi)Z_Q(f) - g\sin(\phi)Z_I(f)] \\ &= [H_I(f) - jg\sin(\phi)H_Q(f)]Z_I(f) + j[g\cos(\phi)H_Q(f)]Z_Q(f) \\ &= A_I(f)Z_I(f) + jA_Q(f)Z_Q(f) \end{aligned} \tag{3–7}$$

where $A_I(f) = [H_I(f) - jg\sin(\phi)H_Q(f)]$ and $A_Q(f) = g\cos(\phi)H_Q(f)$. Now, using the general result of (2–13), $Z'(f)$ can be written as

$$Z'(f) = G_1(f)Z(f) + G_2(f)Z^*(-f) \tag{3–8}$$

where the general imbalance functions $G_1(f)$ and $G_2(f)$ are given by

$$\begin{aligned} G_1(f) &= [H_I(f) + H_Q(f)ge^{-j\phi}]/2 \\ G_2(f) &= [H_I(f) - H_Q(f)ge^{j\phi}]/2. \end{aligned} \tag{3–9}$$

This relationship between the ideal and imbalanced baseband equivalents $z(t)$ and $z'(t)$ is illustrated graphically in Figure 3–4.

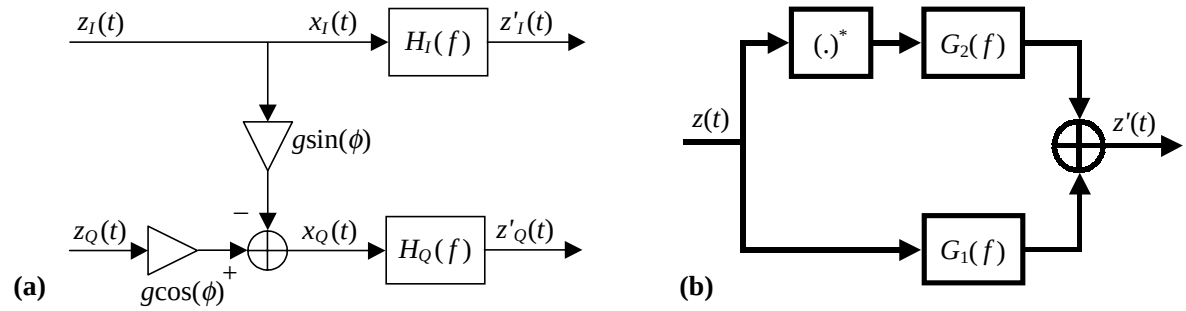

Figure 3–4: *Wideband signal model for front-end imbalances in terms of (a) real-valued and (b) complex-valued signals.*

Clearly, according to (3–8), the combined effect of I/Q mismatches is to cause the image component $z^*(t)$ to appear in addition to the desired component $z(t)$. This result is independent of the actual source of imbalance. As in case of real mixing, imbalanced quadrature mixing also results in two frequency translations. Even though these translations take place with different relative strengths, this already compromises the ideal infinite image

rejection. Then, after the downconversion process, a specific channel centered at f_{IF} has its original image signal located around $-f_{\text{IF}}$ (or vice versa). Thus, since the mismatches in the branch components cause part of the signal energy at any specific band to alias to the corresponding mirror band, the image attenuation capability is further degraded. Based on (3–8), the effective image attenuation of the whole analog front-end is given by

$$L(f) = \frac{|G_1(f)|^2}{|G_2(f)|^2}. \tag{3–10}$$

Clearly, the image attenuation of (3–10) is in general frequency-dependent.

The total mismatch effect as predicted by (3–8) is illustrated graphically in Figure 3–5. Again, the desired signal is depicted in grey and its image signal in dark. Clearly, the front-end processing cannot sufficiently attenuate the strong image band signal and some kind of further processing is needed.

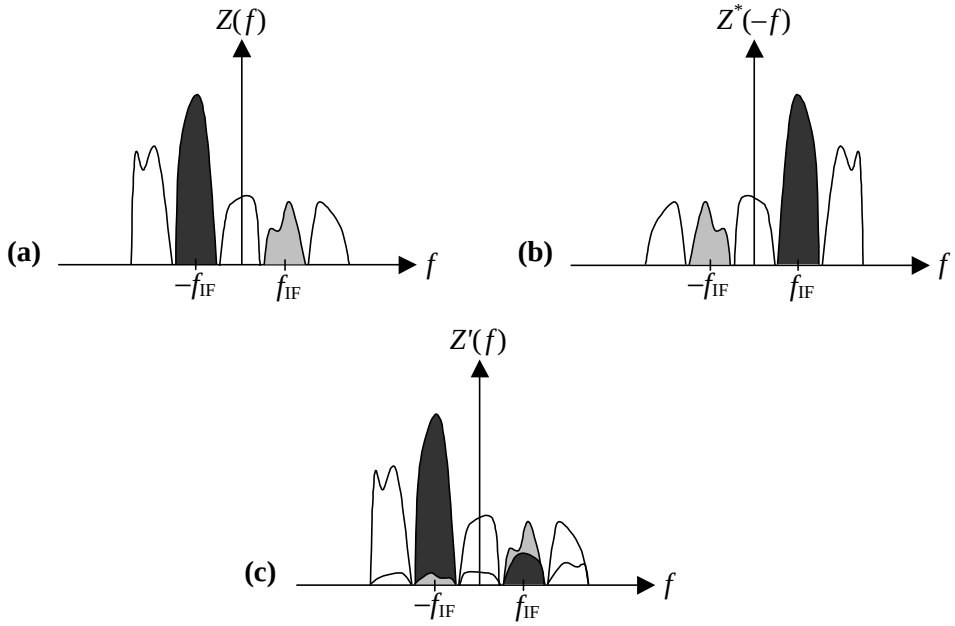

Figure 3–5: *A frequency domain illustration of the basic imbalance effect.*

3.3 Earlier Work on Imbalance Compensation

The task of improving the image signal attenuation of the basic quadrature downconversion scheme, either using analog or digital techniques, has been addressed to some extent in the recent literature. The most common analog techniques based on Hilbert filtering and its approximations are discussed by Crols and Steyaert in [17]-[21]. Several different digital compensation ideas are discussed, e.g., in [9], [10], [24], [29], [30], [31], [53], [65], [66], [68],

[85], [93] by various contributors. Commonly, in the digital methods, the approach is to first estimate the effective mismatches between the I and Q branch amplitudes and phases. Then, employing these estimates, some kind of a correction network is used to restore the ideal matching conditions, i.e., equal amplitudes and a phase difference of 90°. This kind of approaches are in general referred to as the rematching methods. However, most of these methods share the problem of being unable or impractical to compensate for amplitude and phase mismatches which depend on frequency and/or time. Furthermore, most of the proposed estimation techniques are based on known test or calibration signals, complicating their use during the normal receiver operation.

Analog Techniques

In addition to the natural tool of careful circuit design, Hilbert filtering techniques presented in Chapter 2 can be combined with the basic quadrature downconversion scheme to increase the receiver analog image attenuation [20], [21]. This can be understood by observing that only the image signal component at the *negative* frequency band is actually disturbing the desired signal component at positive IF, as presented in Figure 3–5 (c). Now, this destructive image component can be attenuated *before* the quadrature downconversion stage by the Hilbert filtering techniques. What makes this approach more attractive than the traditional real image rejection filtering is the observation that the frequency separation of the image signal component at negative frequencies and the desired signal component at positive frequencies is actually $2f_C$. Clearly, this is much larger than the corresponding frequency separation of $2f_{\mathrm{IF}}$ of a real image rejection filter. Thus, the transition bandwidth of a practical Hilbert approximation, such as the phase splitter, can be much larger than that of a real IR filter hence simplifying its implementation. As a practical example, the front-end phase splitter could reject the image signal by 30 dB, after which another 30 dB could be provided by the quadrature downconversion. This results in a total of 60 dB image attenuation [20], [21]. The practical disadvantage of the above approach is that since the Hilbert filtering already produces a complex-valued signal, fully complex processing is needed in the subsequent quadrature downconversion stage (4 real multiplications and 2 additions). This, in turn, complicates the receiver implementation as a whole. These kind of analog filtering techniques are fully explored, e.g., in [17], [19]-[21].

Digital Techniques

The finite image attenuation of the mismatched analog processing can also be enhanced digitally. Most of the existing digital techniques try to achieve this by rematching the relative

amplitudes and phases of the I and Q branch signals. As the basic starting point, a frequency-independent imbalance model is usually assumed (see, e.g., [24], [29], [82], a frequency-dependent extension is considered in [68]). In our formulation, this means that $z_I'(t) = x_I(t)$ and $z_Q'(t) = x_Q(t)$, and the signal model can be written as

$$\begin{bmatrix} z_I'(t) \\ z_Q'(t) \end{bmatrix} = \begin{bmatrix} 1 & 0 \\ -g\sin(\phi) & g\cos(\phi) \end{bmatrix} \begin{bmatrix} z_I(t) \\ z_Q(t) \end{bmatrix}. \tag{3–11}$$

Then, provided that $g \neq 0$ and $\phi \neq \pm\pi/2$, the model of (3–11) can be inverted as

$$\begin{bmatrix} z_I(t) \\ z_Q(t) \end{bmatrix} = \begin{bmatrix} 1 & 0 \\ \tan(\phi) & (g\cos(\phi))^{-1} \end{bmatrix} \begin{bmatrix} z_I'(t) \\ z_Q'(t) \end{bmatrix}. \tag{3–12}$$

The natural assumptions of $g \neq 0$ and $\phi \neq \pm\pi/2$ simply mean that there really exist two signals (I and Q) which are not phase-aligned. In other words, both the I and Q branches should have a non-zero amplitude ($g \neq 0$) and there should be some phase difference ($\phi \neq \pm\pi/2$) between them.

The use of (3–12) needs to be coupled with proper estimation of the effective amplitude and phase mismatches g and ϕ. Commonly, the proposed estimation methods are based on the availability of known calibration or training signals. When both the ideal and imbalanced signals in (3–11) are known, sampling will basically yield a set of equations which can be solved for the imbalance parameters. Such techniques using a single-frequency sinusoidal calibration signal are presented by Green *et al.* in [31]. The imbalanced I and Q branch signals are sampled and non-linear regression techniques are used to estimate the imbalance parameters. Similar ideas based on a multitone calibration signal and linear regression methods are discussed by Green in [30]. Another closely related approach where the imbalance parameters are estimated using regression techniques is described by Nguyen in [62]. Instead of a sinusoidal calibration signal, a constant amplitude training signal is assumed in [62]. A single-frequency calibration signal is again utilized by Pierre and Fuhrmann in [66] but the actual parameter estimation is carried out in frequency domain. In [29], Glas proposes an estimation scheme for low-IF receivers where two sinusoidal test signals, one at the desired frequency band and another one at the corresponding image band, are used.

An alternative approach to imbalance estimation is introduced by harris in [35]. The idea is to utilize the correlation between the I and Q branch signals caused by the mismatches. Two adaptive loops are used to form the imbalance parameter estimates by forcing the compensated I and Q branch signals to be uncorrelated and of equal amplitudes. A

decorrelator type of compensation structure is also proposed by Cetin *et al.* in [10]. Two adaptive filters are used to provide two uncorrelated sequences. Assuming that the original I and Q branch signals are uncorrelated, the decorrelated signals are used directly as the I and Q signal estimates.

A completely different approach is reported by Lohtia *et al.* in [55]. The idea is to detect the envelope of the quadrature downconverter input signal and use it in estimating the imbalance parameters. Two samples of the envelope are basically needed together with the corresponding samples of the imbalanced I and Q branch signals. This results in a set of two non-linear equations which can be solved for the two unknowns (g and ϕ). The use of envelope eliminates the need for training signals.

In [9], a digital compensation algorithm is proposed for direct-conversion receivers by Cavers and Liao. Due to zero IF, the image signal is effectively the desired signal itself, and imbalances result in a linear distortion of the original signal constellation as given by (3–11). Then, given that a training signal is available, an adaptive equalizer type of compensation structure can be used to restore the undistorted signal constellation. Naturally, this approach is valid as such only for direct-conversion receivers.

In this thesis, in Chapter 4, a novel approach for digital imbalance compensation is introduced. Instead of aiming at restoring the perfect matching conditions, the idea is simply to try to produce a high-quality estimate of the desired channel baseband equivalent signal located at non-zero IF after the initial quadrature downconversion. To accomplish this, statistical signal processing techniques are exploited together with the inherent frequency diversity available in $z'(t)$. In general, this approach is new in the literature of the field. The only contribution in the literature resembling our work is the one reported by Yu and Snelgrove in [93]. Their compensator can be regarded as a decorrelation based signal separator where the basic formulation is carried out for the multichannel signal, i.e., for the signal $z'(t)$ in our notation. While the approach in [93] is mostly heuristic, our results are based on explicit signal models and rest on solid theoretical problem formulation, well-motivated assumptions, and analytical performance results. In general, the results and techniques presented in this thesis and the ideas in [93] were discovered and developed completely independently.

Chapter 4

Statistical Signal Processing Techniques for Imbalance Compensation

In addition to the traditional amplitude and phase rematching methods, the term imbalance compensation is here extended to cover all possible techniques which try to enhance the analog front-end image attenuation of (3–10). More specifically, in our formulation, the target is to obtain an image-free observation of a specific channel (referred to as the desired channel) signal located at a non-zero[7] intermediate frequency after the initial quadrature downconversion stage.

4.1 Two Baseband Observations

In the ideal situation, after perfectly matched I/Q downconversion and lowpass filtering, all the signal energy at the positive and negative intermediate frequencies is contributed by the desired and image signals, respectively. In addition to these signal components, the imbalanced signal $z'(t)$ has a destructive image component at positive IF and also a desired signal component at negative IF as predicted by (3–8). Motivated by this, *two* baseband observations consisting of the desired and image signals can be generated by processing the combined signals around both the negative and positive intermediate frequencies. Then, using these observations, the desired channel signal can be estimated as will be presented in Sections 4.2 and 4.3. First, however, in order to express the proposed compensation ideas in a more formal manner, a baseband signal model for the two observations is derived. Even though all the subsequent processing can in practice be performed digitally, the following analysis is carried out in continuous-time domain for simplicity.

---

[7] In zero-IF receivers, due to the inherent self-image, the image attenuation of a practical analog front-end is, as discussed earlier, likely to suffice for most applications.

To be specific, let $s(t)$ and $i(t)$ denote the baseband equivalents of the desired and image channel signals, respectively. Then, the first observation, say $d(t)$, is obtained simply by translating the combined signal around the *positive* intermediate frequency to baseband. This signal represents the desired channel observation which needs to be generated in any kind of receiver, independently of the front-end matching characteristics. Starting from the general model (3–8), the resulting signal can be expressed in frequency domain as

$$\begin{aligned} D(f) &= Z'(f + f_{\text{IF}})\Pi(f, B_C) \\ &= [G_1(f + f_{\text{IF}})S(f) + G_2(f + f_{\text{IF}})I^*(-f)]\Pi(f, B_C) \end{aligned} \tag{4–1}$$

where B_C denotes the individual channel bandwidth and $\Pi(f, B_C)$ represents the bandlimited filtering function (ideally, $\Pi(f, B_C) = 1$ for $|f| \le B_C/2$ and zero otherwise). Notice that with perfect matching and ideal filtering, the observed signal of (4–1) reduces to $d(t) = s(t)$.

In addition to the desired channel observation $d(t)$, another observation, say $v(t)$, can be generated by demodulating the combined signal around the *negative* intermediate frequency to baseband. For obvious reasons, this signal is referred to as the interference observation. Again, based on (3–8), the resulting signal after spectrum mirroring (complex conjugation) can be written in the frequency domain as

$$\begin{aligned} V(f) &= Z'^*(-f - f_{\text{IF}})\Pi(f, B_C) \\ &= [G_2^*(-f - f_{\text{IF}})S(f) + G_1^*(-f - f_{\text{IF}})I^*(-f)]\Pi(f, B_C). \end{aligned} \tag{4–2}$$

In the special case of ideal filtering and zero imbalance, this interference observation consists of only the conjugated image signal, i.e., $v(t) = i^*(t)$. For analysis purposes, the signals of (4–1) and (4–2) can be conveniently expressed in matrix formulation as a single two-input two-output model as

$$\mathbf{X}(f) = \mathbf{A}(f)\mathbf{S}(f) \tag{4–3}$$

where $\mathbf{X}(f) = [D(f)\ \ V(f)]^T$, $\mathbf{S}(f) = [S(f)\ \ I^*(-f)]^T$, and the matrix $\mathbf{A}(f)$ appears as

$$\mathbf{A}(f) = \begin{bmatrix} G_1(f + f_{\text{IF}}) & G_2(f + f_{\text{IF}}) \\ G_2^*(-f - f_{\text{IF}}) & G_1^*(-f - f_{\text{IF}}) \end{bmatrix} \Pi(f, B_C). \tag{4–4}$$

These two signals $d(t)$ and $v(t)$ constitute the basis for the actual compensation algorithms to be presented in Sections 4.2 and 4.3. Formally, the idea is to estimate $s(t)$ blindly using only the observed signals $d(t)$ and $v(t)$. In other words, the term blind refers here to the fact that no known training signal is needed. A traditional receiver relying solely

on the front-end image rejection only generates the desired channel observation $d(t)$ and uses that directly as an estimate of $s(t)$. In terms of signal-to-interference ratio (SIR), the quality of this trivial estimator is given by

$$SIR_D = \frac{\int_{-B_C/2}^{B_C/2} |G_1(f + f_{IF})|^2 \Phi_S(f)\, df}{\int_{-B_C/2}^{B_C/2} |G_2(f + f_{IF})|^2 \Phi_{I^*}(f)\, df} \tag{4–5}$$

where $\Phi_Z(f)$ denotes the power spectral density of $z(t)$ in general. The result of (4–5) serves as a natural reference when evaluating the performance of more sophisticated techniques in Section 4.4.

A graphical illustration of the previously described baseband observations is given in Figure 4–1. Also shown is a fully digital implementation structure, where the signal $z'(t)$ is directly sampled and all the above-mentioned processing is performed in discrete-time domain. Thus, to emphasize this, discrete-time notations ($d(n)$, $v(n)$, etc.) are used hereafter throughout the rest of this chapter. Notice that since perfect matching can be achieved in digital processing, no excess imbalance effects are expected to occur in practice.

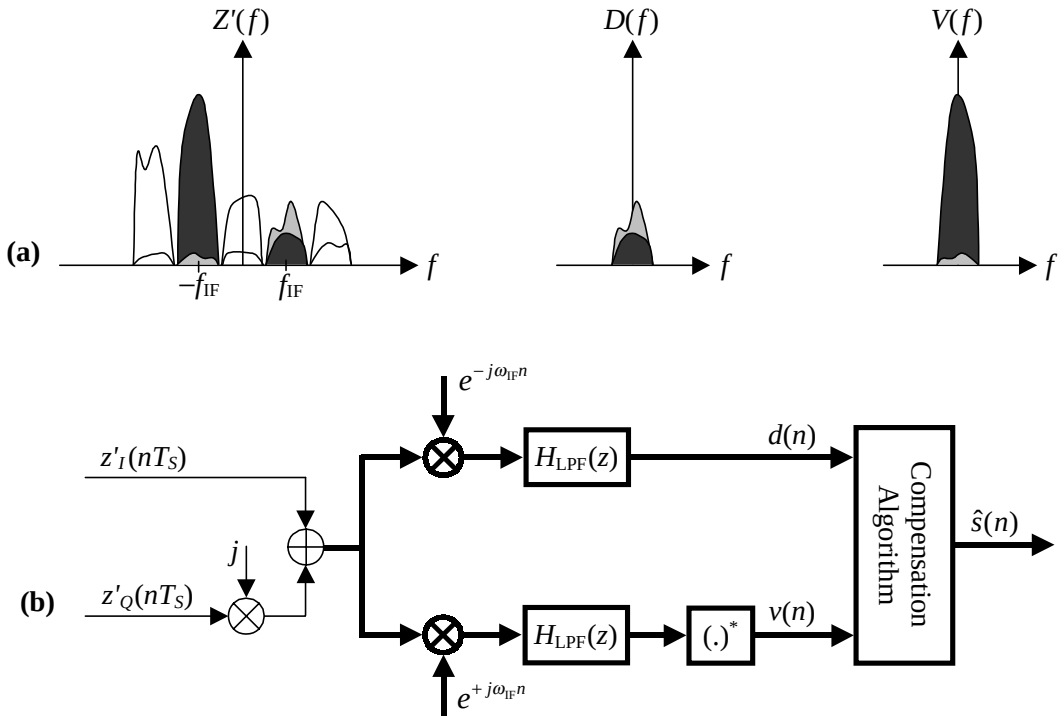

Figure 4–1: *Baseband observation generation for digital imbalance compensation. (a) The spectra of z'(t) and the resulting baseband observations d(t) and v(t). (b) The corresponding digital implementation structure where complex-valued processing is depicted in bold.*

4.2 Interference Cancellation (IC) Based Compensation

Adaptive Interference Cancellation

In adaptive interference cancellation, the primary input signal $d_{\mathrm{PRI}}(n)$ consists of the information-bearing signal of interest corrupted by an uncorrelated additive interference component [36], [90]. In order to improve the signal quality, an estimate of the interfering signal component is subtracted from the primary signal in a controlled manner. This kind of general signal enhancement configuration is illustrated in Figure 4–2. More specifically, the interference estimate is formed by an adaptive filter $w_k(n)$ by employing a reference signal $v_{\mathrm{REF}}(n)$ which is ideally uncorrelated with the information bearing signal but in some way correlated with the interfering noise component. Based on the previous correlation assumptions, the adaptive filter coefficients $w_k(n)$ can be adapted using the primary signal as the desired signal [36], [90]. Thus, the overall system output signal $y(n)$ constitutes directly the error signal for the adaptation process as presented in Figure 4–2. The filter adaptation can be performed with many different adaptive filtering algorithms, such as the well-known least-mean-square (LMS) or recursive least-squares (RLS) algorithms. The choice of the adaptation algorithm leads to different convergence speeds and computational complexities, in general, as well as to different remaining steady-state errors [36], [90].

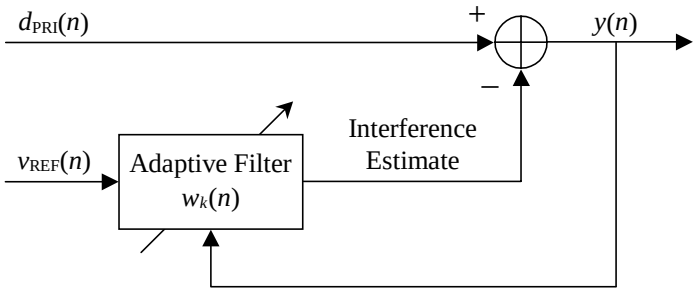

Figure 4–2: *Adaptive interference cancellation.*

Imbalance Compensation

In addition to the desired signal component, the imbalanced desired channel observation $d(n)$ consists also of an interfering image component, as predicted by (4–1). The power ratio of these two components is in general given by (4–5). In practice, compared to the desired signal component, the analog front-end is able to attenuate the image component by 20-40 dB. Thus, if the image signal is originally weak compared to the desired signal, the resulting SIR of (4–

5) will be adequate. In other words, for a weak image signal, the trivial estimator $\hat{s}(n) = d(n)$ will suffice. Therefore, we can focus our attention on the situation where the image signal is more powerful than the desired one.

In case of a strong image signal, the SIR_D of (4–5) is not satisfactory. Then, to enhance the signal quality, the previous interference cancellation techniques can be exploited by simply using $v(n)$ as the reference signal to eliminate the image component of the primary input $d(n)$. Formally, using a finite impulse response (FIR) compensation filter of length $N_{\mathrm{IC}}+1$, the estimate of the desired signal is then given by

$$\hat{s}_{\mathrm{IC}}(n) = d(n) - \sum_{k=0}^{N_{\mathrm{IC}}} w_k(n) v(n-k) . \tag{4–6}$$

The rationale behind this idea is that the power difference of the two signal components of $v(n)$ is the original power difference of the desired and image signals *added* by the analog front-end image attenuation. Thus, in case of a powerful image signal, $v(n)$ is strongly correlated with the interference component but only slightly correlated with the desired signal component of $d(n)$. Given that the receiver imbalance properties do not depend on frequency, a single-tap ($N_{\mathrm{IC}} = 0$) compensation filter can be used. This special case is explored in more detail in Section 4.4.

To be precise, our signal model of (4–3) is not exactly ideal for interference cancellation. This is because the interference observation $v(n)$ has also a small desired signal component resulting in a non-zero correlation between the desired signal $s(n)$ and $v(n)$. Generally, this phenomenon is known as signal leakage [36], [90] and can degrade the system performance. More specifically, if the desired signal is originally stronger than the image signal, the correlation between $v(n)$ and the desired signal component of $d(n)$ cannot be neglected, and the compensation performance starts to deteriorate. This will be characterized in more detail in Section 4.4. In this case, however, $d(n)$ is only slightly interfered by the image signal in the first place and can be used directly as an estimate of $s(n)$. Clearly, this kind of approach requires some kind of estimation of the powers of the different channel signals to decide whether to switch the interference canceller on or off.

4.3 Blind Source Separation (BSS) Based Compensation

Blind Separation of Sources

Given m linear mixtures $x_1(n), ..., x_m(n)$ of $l \le m$ source signals $s_1(n), ..., s_l(n)$, the task of blind source separation is to reproduce the original source contributions. Here, the term *blind* is used to emphasize that the linear mixing system behind the observations is unknown and only the statistical properties of the sources will be exploited. More specifically, a strong but plausible assumption of mutual independence of the original source signals is commonly employed [4], [6], [7], [12], [37], [42], [43], [47].

In general, the multichannel linear mixture model is formulated as

$$\mathbf{x}(n) = \sum_k \mathbf{A}_k \mathbf{s}(n-k) \tag{4–7}$$

where $\mathbf{x}(n) = [x_1(n), ..., x_m(n)]^T$ is an m-column vector of observations, $m \times l$ complex matrices $\mathbf{A}_k$ define the mixture coefficients, and $\mathbf{s}(n) = [s_1(n), ..., s_l(n)]^T$ is an l-column vector of source signal samples[8]. The recovery of the original source signals is in general feasible if $\mathbf{A}(z) = \sum_k \mathbf{A}_k z^{-k}$ has full rank and at most one source signal is Gaussian. For a detailed description and explanation of the general identifiability conditions, see [6] and the references therein. Without any loss of generality, the source signals are usually assumed to have zero mean and unit variance [4], [6], [7], [37].

Adaptive estimation of the source signals is in general performed by a multichannel filtering operation as

$$\mathbf{y}(n) = \sum_k \mathbf{W}_k(n)\mathbf{x}(n-k) = \hat{\mathbf{s}}(n) \tag{4–8}$$

where the $l \times m$ separating matrices $\mathbf{W}_k(n)$ are adapted to minimize some measure of mutual dependence between the separated output signals (components of $\mathbf{y}(n)$). This is illustrated in Figure 4–3. Without any additional information, such as cyclo-stationarity or different spectral contents, on the source signals, higher-order statistics (HOS), such as kurtosis, can and need to be exploited [6], [43], [88]. Furthermore, the sources can only be recovered up to

[8] The term blind source separation refers usually to the instantaneous mixture case where all other matrices except $\mathbf{A}_0$ are all-zero. More generally, if two or more of the matrices $\mathbf{A}_k$ are non-zero, the observed signals appear as convolutive mixtures of the original source signals, and the term multichannel blind deconvolution (MBD) is commonly in use.

permutation, scaling, and delay. In general, there exists a wide variety of different approaches (see, e.g., [37] for an excellent review) to measure the independence of the separated output signals and consequently to adapt the demixing matrices $\mathbf{W}_k(n)$.

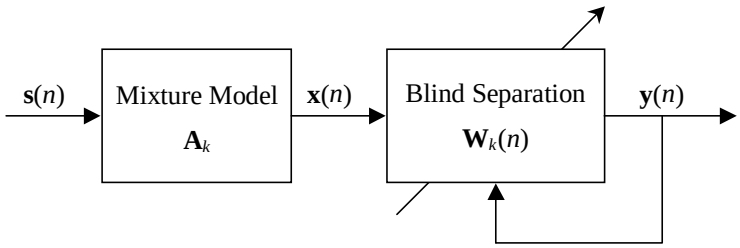

Figure 4–3: *Blind source separation.*

Imbalance Compensation

Based on (4–3), our discrete-time observations $d(n)$ and $v(n)$ appear as convolutive mixtures of the desired and image signals. With a realistic front-end design, the related mixture matrix of (4–4) is invertible or of full rank, as can be easily verified. Then, assuming that the desired and image channel signals are mutually independent, a blind source separation algorithm can be employed in estimating the desired signal $s(n)$ as well as the interfering signal $i(n)$. More specifically, using FIR separation filters of length $N_{\text{BSS}}+1$, the estimate of the source vector $\mathbf{s}(n)=[s(n)\ \ i^*(n)]^T$ can be obtained (up to permutation and scaling) directly as

$$\hat{\mathbf{s}}(n)=\sum_{k=0}^{N_{\text{BSS}}}\mathbf{W}_k(n)\mathbf{x}(n-k) \tag{4–9}$$

where $\mathbf{x}(n)=[d(n)\ \ v(n)]^T$. Then, the actual desired channel signal is estimated as

$$\hat{s}_{\text{BSS}}(n)=\mathbf{e}_i^T\hat{\mathbf{s}}(n),\ \ i=1\text{or }2 \tag{4–10}$$

where $\mathbf{e}_1=[1\ \ 0]^T$ or $\mathbf{e}_2=[0\ \ 1]^T$ is used, depending on the possible source permutation. If the front-end imbalances are frequency-independent, the general signal model of (4–3) reduces to an instantaneous mixture model and a single-tap ($N_{\text{BSS}}=0$) multichannel filter can be used for compensation. This will be described in detail in Section 4.4.

4.4 Performance Results

In order to express the usefulness of the proposed compensation techniques in a more formal manner, some performance results are presented next. The performance measure is the signal-to-interference ratio (SIR) at the output of the compensation structure. For simplicity, we concentrate on the frequency-independent situation for which $H_I(f) = H_Q(f) = 1$, i.e., all the amplitude and phase imbalances are represented by g and ϕ, respectively. Furthermore, for analysis purposes, we study the situation of linearly modulated circularly symmetric[9] communication signals with ideal symbol rate sampling. We also assume that the desired and image signals are wide-sense stationary (WSS), zero mean, i.i.d. sequences that are also independent of each other. Notice, however, that all the previous assumptions on the type of modulation, etc., are made only to make the analysis more feasible. The only fundamental assumptions needed in IC and BSS based imbalance compensation techniques are the mutual uncorrelatedness and independence of the desired and image signals. Since the signals in different frequency bands are likely to arise from physically different sources, these assumptions should be reasonable. Furthermore, since the compensation can be carried out before any modulation-specific processing, the proposed techniques should work with all the standard modulation techniques, such as phase-shift keying (PSK), quadrature amplitude modulation (QAM), Gaussian minimum-shift keying (GMSK), etc. In the following, the performance results are simply stated in a concise manner. More detailed analyses can be found in the original papers [P2]-[P4].

Frequency-Independent Signal Model

With the previous assumptions, we can write the general signal model of (4–3) as an instantaneous mixture model as

$$\mathbf{x}(n) = \begin{bmatrix} d(n) \\ v(n) \end{bmatrix} = \begin{bmatrix} K_1\sqrt{P_S} & K_2\sqrt{P_I} \\ K_2^*\sqrt{P_S} & K_1^*\sqrt{P_I} \end{bmatrix} \begin{bmatrix} s_1(n) \\ s_2(n) \end{bmatrix} = \mathbf{A}\mathbf{s}(n) \tag{4–11}$$

where $P_X = E(|x(n)|^2)$, in general, and the imbalance coefficients K_1 and K_2 are given by (3–2). The effective unit variance source signals are expressible as $s_1(n) = s(n)/\sqrt{P_S}$ and $s_2(n) = i^*(n)/\sqrt{P_I}$. Notice that since $\det(\mathbf{A}) = \sqrt{P_S P_I}(|K_1|^2 - |K_2|^2) = g\cos(\phi)\sqrt{P_S P_I}$, the

[9] In general, a zero mean complex-valued signal $x(n)$ is said to be circularly symmetric or simply circular if $E(x^2(n)) = 0$.

traditional assumptions on the imbalances ($g \neq 0$ and $\phi \neq \pm\pi/2$) are sufficient to guarantee that the model of (4–11) is identifiable, i.e., that $\det(\mathbf{A}) \neq 0$ [6].

With the previous signal model, the quality of the trivial estimator $\hat{s}(n) = d(n)$, as given by (4–5) in the general case, reduces now to

$$SIR_D = \frac{|K_1|^2 P_S}{|K_2|^2 P_I}. \tag{4–12}$$

This fundamental SIR value is referred to as the quadrature limit and it constitutes a natural reference level when evaluating the performance of the IC and BSS based techniques.

Interference Cancellation

By definition, with a single-tap adaptive filter $w_0(n) \equiv w^*(n)$, the IC based estimate of the desired signal $s(n)$ can be written as $y(n) = d(n) - w^*(n)v(n) = \hat{s}_{\mathrm{IC}}(n)$. Then, using (4–11), this can be expressed as

$$\begin{aligned} y(n) &= \left(K_1 - w^*(n)K_2^*\right)\sqrt{P_S}\, s_1(n) + \left(K_2 - w^*(n)K_1^*\right)\sqrt{P_I}\, s_2(n) \\ &= c_1(n)s_1(n) + c_2(n)s_2(n). \end{aligned} \tag{4–13}$$

Clearly, the fixed optimum solution for which $c_2(n) = 0$ is $w_{\mathrm{OPT}} = K_2^*/K_1$.

Based on (4–13), the average SIR can now be defined as

$$SIR_{\mathrm{IC}} = \frac{E(|c_1(n)|^2)}{E(|c_2(n)|^2)}. \tag{4–14}$$

The fixed minimum mean-squared error (MSE) solution denoted by w_{MSE} is obtained by minimizing $J_{\mathrm{MSE}} = E(|y(n)|^2)$. The resulting SIR is given by

$$SIR_{\mathrm{IC}}^{\mathrm{MSE}} = \frac{|K_1|^2 P_I}{|K_2|^2 P_S} = \frac{1}{SIR_V} \tag{4–15}$$

where SIR_V is the signal-to-interference ratio in the reference signal $v(n)$. Thus, due to a small desired signal component in the interference observation, the performance of MSE based solutions is bounded as stated in (4–15). In other words, interference cancellation is not perfect and some interference will always remain. However, since $P_I >> P_S$ implies $SIR_{\mathrm{IC}}^{\mathrm{MSE}} >> SIR_D$, (4–15) gives a formal justification for the validity of IC based compensation in case of a strong image signal.

The practical LMS algorithm is a simple approximation of the iterative steepest-descent (SD) optimization technique [36], [90]. More specifically, the idea in the LMS algorithm is to try to minimize the MSE recursively using instantaneous sample estimates of the gradient of the mean-squared error surface. Denoting the LMS filter coefficient by $w_{\mathrm{LMS}}(n)$, the resulting SIR can be expressed as

$$SIR_{\mathrm{IC}}^{\mathrm{LMS}} = \frac{\left(|J_1|^2 + |K_2|^2\, E(|\varepsilon(n)|^2)\right)P_S}{\left(|J_2|^2 + |K_1|^2\, E(|\varepsilon(n)|^2)\right)P_I} \tag{4–16}$$

where $\varepsilon(n) = w_{\mathrm{LMS}}(n) - w_{\mathrm{MSE}}$ and

$$\begin{aligned} J_1 &= \frac{K_1 P_I\left(|K_1|^2 - |K_2|^2\right)}{|K_1|^2\, P_I + |K_2|^2\, P_S} \\ J_2 &= \frac{K_2 P_S\left(|K_2|^2 - |K_1|^2\right)}{|K_1|^2\, P_I + |K_2|^2\, P_S}. \end{aligned} \tag{4–17}$$

By using the circularity assumption (i.e., assuming that the signals are circularly symmetric), the steady-state value for $E(|\varepsilon(n)|^2)$ can then be written as

$$E(|\varepsilon(n)|^2) = \frac{\mu^2 J_\varepsilon}{1-(1-\mu P_V)^2} \tag{4–18}$$

where μ is the LMS adaptation step-size and

$$\begin{aligned} J_\varepsilon = {} & |K_2 J_1|^2\, E(|s(n)|^4) + |K_1 J_2|^2\, E(|i(n)|^4) \\ & + P_S P_I\left(|K_1 J_1|^2 + |K_2 J_2|^2 + 2\,\mathrm{Re}[K_1 K_2^* J_1^* J_2]\right). \end{aligned} \tag{4–19}$$

Even though the previous results are here formulated for the LMS update, (4–16) and (4–17) actually hold (under the same assumptions) for *any algorithm* for which $E(w(n)) = w_{\mathrm{MSE}}$. The value of $E(|\varepsilon(n)|^2)$ is, of course, highly dependent on the selected adaptation algorithm. Also the convergence rate at which the steady-state solution is approached depends strongly on the selected algorithm [36]. In general, the results of (4–18) and (4–19) hold for any circularly symmetric signal. Only the fourth moments in (4–19) are modulation-specific.

Another commonly used approach in adaptive filtering applications is based on the principle of weighted least-squares (WLS). Using our notations, the WLS solution denoted by w_{WLS} is obtained by minimizing $J_{\mathrm{WLS}} = \sum_{i=1}^{M} \lambda^{M-i} |y(i)|^2$ where $y(n) = d(n) - w^*(n)v(n)$ $= \hat{s}_{\mathrm{IC}}(n)$ and M denotes the amount of available data samples. The exponential weighting

factor λ is limited as $0 < \lambda \leq 1$ with $\lambda = 1$ corresponding to the ordinary least-squares (LS) solution. In general, the solution w_{WLS} is characterized by the well-known normal equations [36] and is in our case of the form

$$w_{\mathrm{WLS}} = \frac{\sum_{i=1}^{M} \lambda^{M-i} v(i) d^*(i)}{\sum_{i=1}^{M} \lambda^{M-i} v(i) v^*(i)}. \tag{4–20}$$

In practice, the WLS solution can be calculated sequentially in time using the well-known recursive least-squares (RLS) algorithm [36]. Since $d(n) = w_{\mathrm{OPT}}^* v(n) + e_0(n)$ where $w_{\mathrm{OPT}} = K_2^* / K_1$ and $e_0(n) = K_1(1 - |K_2|^2 / |K_1|^2) s(n)$, the solution given by (4–20) can also be written as

$$w_{\mathrm{WLS}} = w_{\mathrm{OPT}} + \frac{\sum_{i=1}^{M} \lambda^{M-i} v(i) e_0^*(i)}{\sum_{i=1}^{M} \lambda^{M-i} v(i) v^*(i)}. \tag{4–21}$$

Intuitively, for $\lambda = 1$ and uncorrelated $v(n)$ and $e_0(n)$, the numerator in the coefficient error term in (4–21) is vanishingly small and $w_{\mathrm{WLS}} \approx w_{\mathrm{OPT}}$. In our case, however, $v(n)$ and $e_0(n)$ are *not* uncorrelated since they both contain signal components relative to the desired signal $s(n)$ (signal leakage). Thus, the WLS solution w_{WLS} is expected to contain some error or bias with respect to the optimum solution w_{OPT}. Notice, however, that any further statistical analysis of this error (and the resulting SIR) is extremely difficult to carry out analytically due to correlation between $v(n)$ and $e_0(n)$ [36].

Blind Source Separation

Starting from (4–9) and (4–11) and using the notation $\mathbf{W}_0(n) \equiv \mathbf{W}(n)$, the output signal $\mathbf{y}(n) = \mathbf{W}(n)\mathbf{x}(n) = \hat{\mathbf{s}}(n)$ of the BSS based compensator can be written as

$$\mathbf{y}(n) = \mathbf{W}(n)\mathbf{A}\mathbf{s}(n) = \mathbf{C}(n)\mathbf{s}(n). \tag{4–22}$$

Then, since $y_1(n) = C_{11}(n)s_1(n) + C_{12}(n)s_2(n)$ and $y_2(n) = C_{21}(n)s_1(n) + C_{22}(n)s_2(n)$, the output signal-to-interference ratios can be defined as

$$SIR_{\mathrm{BSS},1} = \frac{E(|C_{11}(n)|^2)}{E(|C_{12}(n)|^2)}, \quad SIR_{\mathrm{BSS},2} = \frac{E(|C_{22}(n)|^2)}{E(|C_{21}(n)|^2)} \tag{4–23}$$

where $C_{ij}(n) = [\mathbf{C}(n)]_{ij}$. Formally, without source permutation, $SIR_{\mathrm{BSS},1}$ corresponds to the SIR of the desired signal estimate $\hat{s}_{\mathrm{BSS}}(n) = y_1(n)$ and thus measures the compensation

performance. For permuted source signal estimates, on the other hand, $\hat{s}_{\mathrm{BSS}}(n) = y_2(n)$ and the definitions of (4–23) should be inverted.

Naturally, the SIR behaviour depends heavily on the selected update rule. In this context, the concept of equivariance is of relevance if the separation performance is independent of the actual mixture parameters. The family of equivariant adaptive separation via independence (EASI) algorithms [6], [7] perform the adaptation serially as

$$\mathbf{W}(n+1) = \big(\mathbf{I} - \alpha(n)\mathbf{H}(\mathbf{y}(n))\big)\mathbf{W}(n) \tag{4–24}$$

where $\alpha(n)$ is the learning or step-size parameter and $\mathbf{I}$ denotes an identity matrix of proper dimensions. The matrix-valued adaptation function $\mathbf{H}(\cdot)$ is in general of the form

$$\mathbf{H}(\mathbf{y}) = \mathbf{y}\mathbf{y}^H - \mathbf{I} + \mathbf{f}(\mathbf{y})\mathbf{y}^H - \mathbf{y}\mathbf{f}(\mathbf{y})^H \tag{4–25}$$

where $\mathbf{f}(\cdot) = [\, f_1(\cdot) \quad f_2(\cdot)]^T$ and $f_i(\cdot)$ are zero-memory non-linear functions. The separation capability stems from cancelling non-linear cross-correlations between the separated output signals. The $\mathbf{y}\mathbf{y}^H - \mathbf{I}$ part in (4–25) is the "whitening" part which ensures that the separated signals are uncorrelated and have unit variance. Depending on whether the source signals are sub-Gaussian (negative kurtosis[10]) or super-Gaussian (positive kurtosis[10]), third-order and hyperbolic tangent type of non-linear functions $f_i(\cdot)$ can be used [6], [7]. In the following, due to the assumption of linearly modulated and circular communications signals, standard cubic non-linearities of the form

$$f_i(y_i) = y_i \,|\, y_i \,|^2 , \quad i = 1, 2 \tag{4–26}$$

are being used.

In general, using the non-linear functions of (4–26), the compensation performance of the EASI algorithm depends on the non-linear source moments of the form [6], [7]

$$\begin{aligned} \kappa_i &= 2E(|\, s_i(n)\,|^2) - E(|\, s_i(n)\,|^4) , \quad i = 1, 2 \\ \gamma_i &= E(|\, s_i(n)\,|^6) - [E(|\, s_i(n)\,|^4)]^2 , \quad i = 1, 2 . \end{aligned} \tag{4–27}$$

Then, based on the circularity and unit variance assumptions, it follows directly that $\kappa_i = 2 - E(|\, s_i(n)\,|^4) = -\mathrm{kurt}(s_i(n))$ where $\mathrm{kurt}(s_i(n))$ denotes the kurtosis of $s_i(n)$. Thus, for

[10] The kurtosis of a zero mean complex-valued signal $x(n)$ is here defined as

$$\mathrm{kurt}(x(n)) = E(|\, x(n)\,|^4) - 2\,[E(|\, x(n)\,|^2)]^2 - |\, E(x^2(n))\,|^2 .$$

any modulation method with constant envelope signals, such as M-ary PSK (M-PSK), $\kappa_i = 1$ and $\gamma_i = 0$ and the SIR measures of (4–23) approach $4/\alpha$ in the steady-state.

Numerical Examples and Simulations

To illustrate and concretize the previous results, some computer simulations are carried out. In the simulations, both the desired and image signals are drawn from two quaternary PSK (QPSK) modulators and the baseband observations $d(n)$ and $v(n)$ are generated according to the basic signal model (4–11) with symbol rate sampling. The imbalance parameters are set to 2% and $2°$ corresponding to an equivalent of 34 dB analog front-end image attenuation. The value of original SIR (P_S / P_I) ranges from -80 dB to 0 dB. To make the situation more practical, some additive noise and symbol timing error (raised-cosine pulse-shape, roll-off factor 0.35) are also included. More specifically, the interferer timing error is zero and the desired signal's timing error is half of the symbol period. In general, ensemble averaging is carried out through 100 independent trials.

The steady-state SIR performance of the interference canceller based compensation technique is presented in Figure 4–4 using both the LMS and RLS algorithms. In the simulations, the LMS adaptation step-size $\mu = 10^{-3} / P_V$ and the RLS relative weighting factor $\lambda = 1$. The corresponding signal-to-interference ratio with the minimum MSE compensator ($SIR_{\mathrm{IC}}^{\mathrm{MSE}}$) is also depicted for reference together with the quadrature limit SIR_D. Evidently, with the selected adaptation parameters ($\mu = 10^{-3} / P_V$ and $\lambda = 1$), SIR in the order of 30 … 40 dB is in general feasible. Despite the additive noise and timing error, the simulated SIR performance of the LMS algorithm is close to the theoretical value of (4–16). Thus, the IC based method proves to be insensitive to additive noise and timing errors. In these example simulations, the RLS algorithm results in approximately 8 dB better SIR performance than the LMS algorithm. On one hand, in order to limit the memory of the RLS algorithm (e.g., for tracking purposes), $\lambda < 1$ can be used in practice. This decreases the RLS steady-state SIR. On the other hand, the LMS steady-state SIR can always be increased closer to the minimum MSE limit $SIR_{\mathrm{IC}}^{\mathrm{MSE}}$ by reducing the step-size μ. The price to pay is, of course, reduced convergence speed. For detailed analyses of the general tracking capabilities of the LMS and RLS algorithms, see [36].

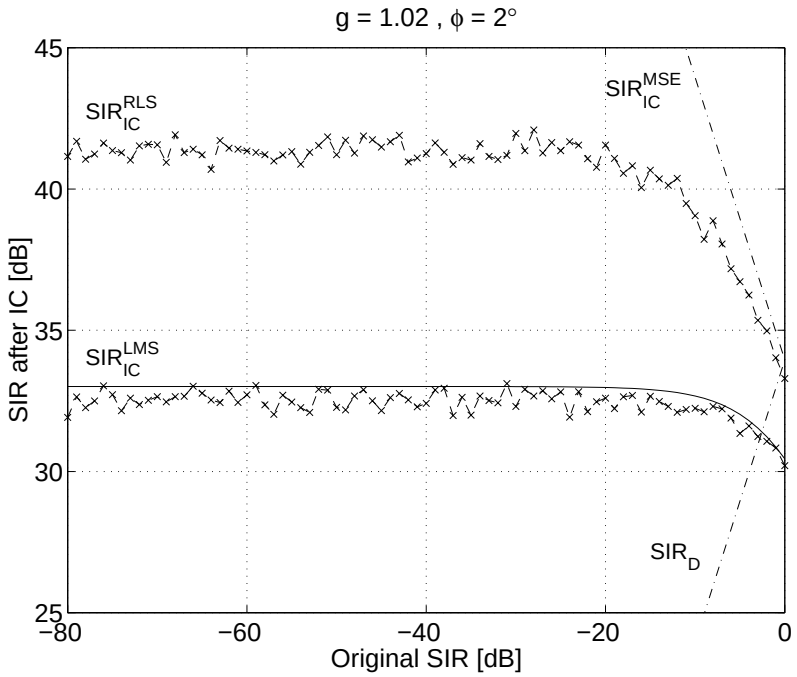

Figure 4–4: *Theoretical (solid) and simulated (x-marked) interference canceller steady-state SIR performances,* $\mu P_V = 10^{-3}$ *(LMS) and* $\lambda = 1.0$ *(RLS). Both the desired and image signals are QPSK modulated, timing error of half of the symbol interval and additive noise of SNR* = 10 *dB included .*

The SIR performance of the EASI algorithm based blind source separator is presented in Figure 4–5, verifying satisfactory steady-state operation. In the simulations, the EASI adaptation step-size $\alpha = 0.002$. With this value, the steady-state SIR is comparable to the SIR of the LMS-IC compensator reported in Figure 4–4. Notice that the inherent signal leakage phenomenon of the IC technique is here avoided. Naturally, the steady-state SIR can be increased by using a smaller adaptation step-size α. This has, however, the obvious drawback of reducing the convergence speed. While the effect of additive noise on the steady-state SIR is clearly marginal, at least at the selected noise level, the symbol timing error affects the operation dramatically. The fundamental reason for this is that the timing errors change the statistical properties of the effective source signals. This phenomenon is addressed analytically in [S2]. The worst situation happens when the interferer timing error is zero and the desired signal's timing error is half of the symbol period. Here, with the selected cubic non-linearity, the degradation is approximately 5 dB. To combat the effects of timing errors, a more robust non-linearity than the basic 3rd order function of (4–26) is proposed in [S2]. A detailed comparison of the IC and BSS based methods is given in Section 4.5. Much more simulation results related to both the steady-state operation and the convergence properties can be found in publications [P1]-[P5].

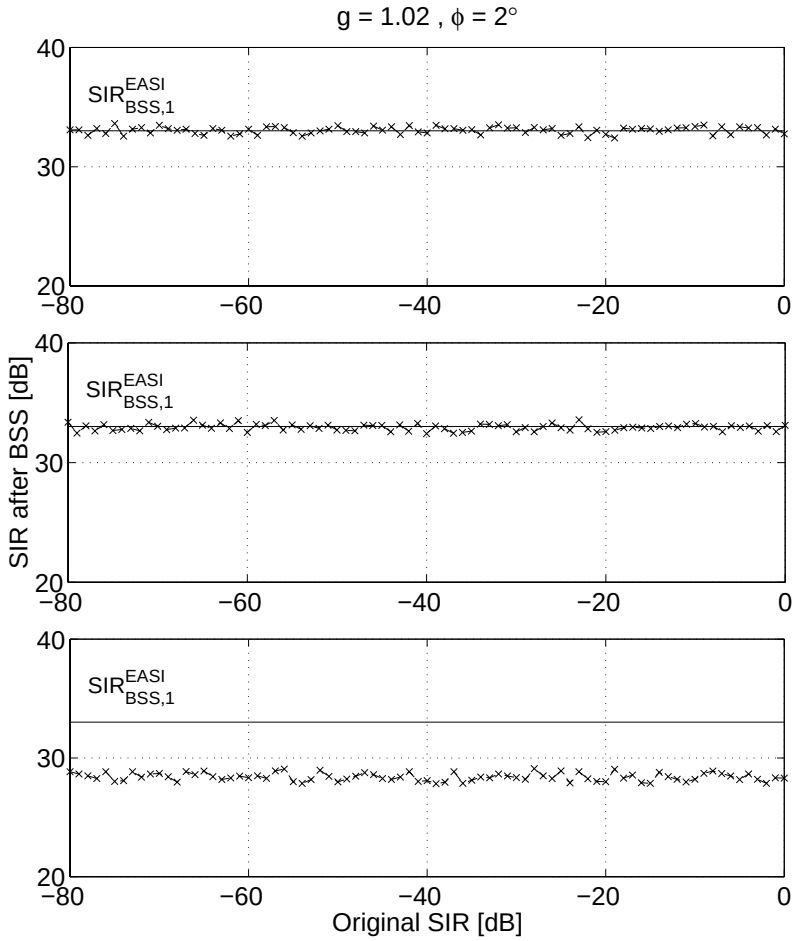

Figure 4–5: *Theoretical (solid) and simulated (x-marked) signal separator steady-state SIR performances,* α = 0.002 *(EASI). Both the desired and image signals are QPSK modulated, (a) ideal sampling and no additive noise, (b) ideal sampling and additive noise SNR* = 20 *dB, and (c) half of the symbol interval timing error and additive noise SNR* = 20 *dB.*

4.5 Comparisons and Practical Matters

The basic requirement in the development of the interference cancellation based compensator was that the desired and interfering signals should be uncorrelated. The source separation based compensator, on the other hand, implicitly assumes the statistical independence of the desired and interfering signals and is generally based on the use of higher-order statistics. A clear advantage of the BSS based compensator is that its performance is extremely robust to the different receiver imbalance properties and to different received signal levels given that the assumed signal model is valid. Also, the signal leakage problem inherent to the interference canceller is avoided though in case of a powerful desired signal, no digital compensation algorithm is likely to reach the performance of the trivial estimator $\hat{s}(n) = d(n)$ in practice. The IC based method, in turn, is more robust to the effects of additive noise and

especially to the effects of symbol timing errors than the BSS based technique. This is explored analytically in the supplementary paper [S2]. Furthermore, the IC based compensator may be less sensitive to the modulation method and to the type of the interfering signal than the BSS based compensator. This is, however, only due to possible limitations of the individual separation algorithms, such as the EASI algorithm, not to the BSS principle itself. This can be affected by a proper algorithm selection and initialization (choice of the non-linearities, etc.). If the receiver imbalance properties depend on frequency, the IC based compensator is directly applicable by using a multitap compensation filter. In that kind of situations, also the source separation based methods are applicable in the form of convolutive mixture separation techniques. These are discussed in detail in [P5].

Stemming from the basic adaptive formulation, both the IC and BSS based methods are able to track the time-variations of the receiver imbalance properties. The LMS-IC algorithm is likely to be able to follow the changes in the analog parameters, e.g., due to temperature variations. However, fast convergence of the RLS-IC algorithm may be needed, e.g., in mobile communications where the changes in the operating conditions of the analog front-end can result in rapidly changing imbalance. As an example, fast changes in the operating frequency in frequency-hopping systems could cause sudden changes in the front-end imbalance properties. As verified by computer simulations (see, e.g., [P4]), the BSS based compensator utilizing, e.g., the EASI algorithm is also able to adapt rapidly to time-varying imbalances.

Due to the inherent matrix processing and involved non-linearities, the computational complexity and storage requirements of the BSS based compensators are in general higher than those of the IC based compensators. Naturally, the exact complexities of the IC and BSS based methods depend on the selected adaptation and update rules. With a single-tap adaptive filter, the computational complexities of the LMS-IC and RLS-IC algorithms are comparable. Notice, however, that the basic RLS update always includes a division operation but the LMS does not [36]. Much more details on the computational complexities can be found, e.g., in [36] and [37].

The fundamental assumption in deriving the basic signal models was that the front-end operation can be modelled as a linear system. In practical implementations, the non-linearities cannot be avoided. Clearly, due to intermodulation distortions, etc., this may reduce the performance of the proposed compensation techniques. However, the ability to perform the compensation using true-world measured low-IF receiver front-end signals is established in the supplementary paper [S3]. Based on the reported results, though preliminary, the studied algorithms can perform the compensation also in practical signal environments.

4.6 System-Level Aspects

The basic application of the proposed imbalance compensation techniques is in a single-channel receiver where the desired channel signal is quadrature downconverted to a non-zero intermediate frequency. Then, the analog front-end image rejection can be enhanced digitally as proposed in Sections 4.1 - 4.3. This approach is, however, also applicable in wideband receivers where a collection of desired signals is downconverted as a whole. In that case, by selecting the individual intermediate frequencies to be integer multiples of the channel bandwidth, the compensation can simply be carried out on a channel-by-channel basis. In other words, for each pair of mirror channels, two baseband observations are generated and used as input signals to a digital algorithm. Thus, the complex-valued processing of Figure 4–1 (b) needs to be implemented for all the signal pairs located at $\pm f_{\mathrm{IF}}^{1}$, $\pm f_{\mathrm{IF}}^{2}$, etc. Naturally, if any of the desired signals is much stronger than its mirror signal, the powerful signal can rely only on the analog front-end image rejection and digital enhancement is needed only for the weak one. Also, if the mirror channel pair consists of equally strong signals, the image attenuation of the analog front-end is likely to suffice for them both.

Chapter 5

Bandpass Sampling and Quadrature Demodulation

In periodic sampling, the resulting discrete-time signal has a periodic spectrum where the original continuous-time spectrum is repeated around the integer multiples of sampling frequency. Interestingly, any of these spectral replicas ("images") can be considered as the useful part and thus be used for further processing. Consequently, bandpass sampling and multirate operations in general can be used, in addition to mixing techniques, in performing frequency translations [15], [16], [86].

5.1 Sampling of Bandpass Signals

Again, as in the previous chapters, we assume that the received signal $r(t)$ is formally expressible as given in (2–1) and (2–2). Furthermore, the lowpass equivalent $z(t)$ (and thus the received signal) is assumed to be strictly bandlimited to a bandwidth B (i.e., $Z(f) \neq 0$ only for $-B/2 \leq f \leq B/2$).

In the following, sampling rate requirements for alias-free sampling of bandpass signals are formulated. In general, the sampling frequency is denoted by $f_S = 1/T_S$. Naturally, aliasing can always be avoided by simply using $f_S \geq 2f_C + B$ which represents the Nyquist frequency. However, due to the bandpass nature of the signal to be sampled, it is also possible to use a sampling frequency below this traditional Nyquist frequency, and still avoid aliasing on top of the useful signal band. In other words, aliasing is allowed and will take place but only in a controlled manner in such a way that all the information in the original bandpass signal is still present in the resulting sample stream. This kind of approaches are generally known as subsampling or simply bandpass sampling techniques [15], [16], [22], [25], [54], [86].

Real Sampling

In real subsampling, not all the values of f_S below the Nyquist frequency are allowed. In general, the usable sampling frequencies depend on both the bandwidth B and the center-frequency f_C. These alias-free sampling frequency regions are expressible as [86]

$$\frac{2f_C + B}{k+1} \le f_S \le \frac{2f_C - B}{k}. \tag{5–1}$$

In (5–1), the integer k is bounded as $0 \le k \le \lfloor R \rfloor$ where $R = (2f_C - B)/(2B)$ and $\lfloor x \rfloor$ denotes the largest integer less than or equal to x. Notice that the traditional Nyquist sampling theorem is just a special case of (5–1) for which $k = 0$. The actual subsampling cases are obtained for $1 \le k \le \lfloor R \rfloor$.

In general, based on the bandwidth assumption ($Z(f) \neq 0$ only for $-B/2 \le f \le B/2$), the ultimate lower limit for alias-free sampling in real sampling is $f_S = 2B$. However, as predicted by (5–1), this minimum sampling frequency is usable only if R is an integer, i.e., only if $2f_C - B = 2kB$. Notice also that in real subsampling, it is not possible to use aliasing to translate any part of the useful band directly to baseband.

Complex or I/Q Sampling

The above constraints of real subsampling can be readily relaxed by using the concept of complex or I/Q sampling [33], [82]. The idea is to sample an analytic signal obtained by a Hilbert transformer, resulting in two sample streams $I(n) = r(nT_S)$ and $Q(n) = \hat{r}(nT_S)$. Now, since the spectrum of $r(t) + j\hat{r}(t)$ is non-zero only for $f_C - B/2 \le f \le f_C + B/2$, a sampling frequency of $f_S = B$ on both branches is always sufficient to avoid harmful aliasing, independently of the center-frequency f_C. Naturally, this results in real-valued samples at rate $2B$. Thus, in terms of the resulting minimum amount of real-valued data samples, I/Q sampling scheme is more efficient than the real sampling as characterized by the ratio

$$S = \frac{2B}{(2f_C + B)/(\lfloor R \rfloor + 1)} = \frac{\lfloor R+1 \rfloor}{R+1} \le 1. \tag{5–2}$$

The concept of I/Q sampling is in general illustrated in Figure 5–1 (a).

Based on (2–2) and (2–7), the signal $r(t) + j\hat{r}(t)$ can also be written as $2z(t)e^{j2\pi f_C t}$. Then, given that the subsampling ratio $r = f_C / f_S$ is an integer, I/Q sampling will result in a direct bandpass-to-lowpass transformation. To see this, the resulting complex-valued sample

sequence can be written as $2z(nT_S)e^{j2\pi f_C nT_S} = 2z(nT_S)e^{j2\pi nr} = 2z(nT_S)$. More formally, in terms of the I and Q branch signals, this can be expressed as

$$\begin{aligned} I(n) &= r(nT_S) = 2z_I(nT_S)\cos(2\pi nr) - 2z_Q(nT_S)\sin(2\pi nr) = 2z_I(nT_S) \\ Q(n) &= \hat{r}(nT_S) = 2z_I(nT_S)\sin(2\pi nr) + 2z_Q(nT_S)\cos(2\pi nr) = 2z_Q(nT_S)\,. \end{aligned} \tag{5–3}$$

Thus, provided that $f_S = f_C / r \geq B$, I/Q subsampling operating on $r(t)$ provides directly an alias-free discrete-time observation of the baseband equivalent $z(t) = z_I(t) + jz_Q(t)$. In the frequency domain, this simply means that the center-frequency of the *r*-th spectral replica will coincide with the zero frequency and that the consecutive replicas will not overlap. This is illustrated in Figure 5–1 (b) for the minimum sampling frequency $f_S = B$. In general, the "digital angular frequency" variable is $\omega = 2\pi f / f_S$.

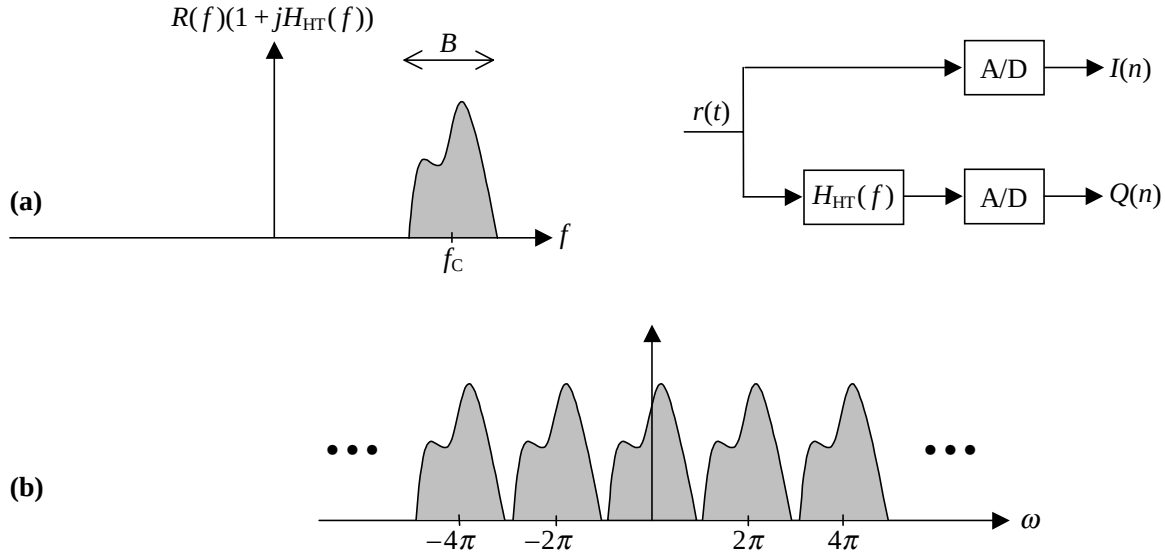

Figure 5–1: *(a) Formal representation of complex or I/Q sampling. (b) The resulting periodic spectrum of the sampled complex-valued signal I(n) + jQ(n) for* $f_S = B = f_C/r$.

5.2 Second-Order Sampling

In practice, implementing a continuous-time and possibly wideband Hilbert transformer needed in the basic I/Q sampling scheme is difficult. Thus, some special means are needed to efficiently approximate this function. With proper parameter values, the general concept of second-order sampling [16], [22], [25] fits directly into this framework.

In general, the second-order sampling of a bandpass signal $r(t)$ consists of two separate sample streams $r(nT_S - \Delta T_1)$ and $r(nT_S - \Delta T_2)$ where $f_S = 1/T_S \geq B$ is the sampling

frequency of both sample streams. To relate this formulation to the previous I/Q sampling and quadrature demodulation, a convenient choice for the sampling time offsets ΔT_1 and ΔT_2 is to use $\Delta T_1 = 0$ and $\Delta T_2 = 1/(4 f_C) = \Delta T$. Then, given that the subsampling ratio $r = f_C / f_S$ is again an integer, the resulting discrete-time sample sequences can be written as

$$\begin{aligned} I'(n) &= r(nT_S) = 2z_I(nT_S) = z'_I(nT_S) \\ Q'(n) &= r(nT_S - \Delta T) = 2z_Q(nT_S - \Delta T) = z'_Q(nT_S). \end{aligned} \tag{5–4}$$

Clearly, also the second-order sampling scheme is able to transform the received bandpass signal directly to baseband. However, the complex-valued discrete-time observation $z'(nT_S) = 2z_I(nT_S) + j2z_Q(nT_S - \Delta T)$ is *not* a perfect reconstruction of the desired baseband equivalent $z(nT_S)$ due to the small but not insignificant relative timing offset ΔT. More specifically, the second-order sampling scheme is *not* able to reject all the signal components from the negative frequencies, resulting in incomplete image rejection. Especially, in case of wideband multichannel signals, this phenomenon cannot be neglected. However, with proper additional discrete-time processing, the demodulation performance of the basic second-order sampling scheme can be enhanced dramatically. This issue will be explored next in detail in Chapter 6.

Chapter 6

Digitally Enhanced Second-Order Sampling Scheme

To form the basis for digitally enhanced second-order sampling techniques, an explicit characterization of the effect of the relative timing offset ΔT is first derived. Again, the emphasis is on techniques suitable for wideband multichannel downconversion. Also, a relation between the ideal I/Q sampling of Section 5.1 and the second-order sampling (or approximative I/Q sampling as it is sometimes referred to as) of Section 5.2 is established. This links nicely together the general imbalance analysis and modelling presented in Chapters 2-4 and the special sampling techniques of Chapters 5 and 6.

6.1 Continuous-Time System Model and Image Attenuation

Hilbert Approximation

Clearly, for the purpose of analysis, the sampling time difference of ΔT between the I and Q branches can be modelled by delaying the Q branch signal with respect to the I branch signal *before* sampling. In other words, the ideal I/Q sampling scheme of Figure 5–1 can be used to model also the second-order sampling scheme by simply replacing the Hilbert transformer by a delay element. Thus, the complex-valued continuous-time equivalent signal behind the second-order sampling scheme of (5–4) is expressible as $r(t)+jr(t-\Delta T)$. To relate this signal to the ideal Hilbert based signal $r(t)+j\hat{r}(t)$, we write its Fourier transform as $[1+jH_{\mathrm{D}}(f)]R(f)$ where

$$[1+jH_{\mathrm{D}}(f)]=1+je^{-j2\pi f\Delta T} \tag{6–1}$$

and $H_{\mathrm{D}}(f)=e^{-j2\pi f\Delta T}$ denotes the frequency response of time delay ΔT. A straight-forward comparison of (6–1) and the corresponding Hilbert based response of (2–7) reveals that

$1+jH_{\mathrm{D}}(f)$ is a very crude approximation of $1+jH_{\mathrm{HT}}(f)$, and the delay processing *cannot* attenuate all the negative frequency components. Actually, the response of (6–1) will match the response of (2–7) only at $f=\pm f_C$. Thus, when $r(t)+jr(t-\Delta T)$ is subsampled at $f_S=f_C/r$, the remaining negative frequency components will alias directly on top of the desired positive frequency components, resulting in incomplete image rejection. This is exactly what happens in the second-order sampling approach. In other words, the second-order sampling scheme is actually quite a poor estimate of I/Q sampling. This will be characterized in a more formal manner in the next subsection.

Another way to look at the situation is through the phase-shifting characteristics. The Hilbert filter simply shifts the phase of the positive frequency components by $-90°$ and the negative frequency components by $+90°$. The delay element, on the other hand, introduces a frequency-dependent phase difference

$$\Delta\Phi=-2\pi f\Delta T=-\frac{\pi}{2}\frac{f}{f_C}. \tag{6–2}$$

This equals the ideal Hilbert behaviour of $\mp 90°\,(\mp\pi/2)$ only at $f=\pm f_C$.

Image Attenuation Analysis

Based on (5–4), it is obvious that the discrete-time signals produced by the second-order sampling can be formally obtained by sampling the corresponding continuous-time equivalent

$$z'(t)=2z_I(t)+j2z_Q(t-\Delta T). \tag{6–3}$$

To see better the destructive effect of the timing difference ΔT, the result of (6–3) can also be written as $z'(t)=z(t)+z(t-\Delta T)+z^*(t)-z^*(t-\Delta T)$. Now, even if ΔT were small, the difference term $z^*(t)-z^*(t-\Delta T)$ will not vanish. In other words, in addition to the desired signal component, $z'(t)$ will contain also an image signal component.

In order to formally characterize the image attenuation capability of (6–3), the Fourier transform of $z'(t)$ can first be written as $Z'(f)=2Z_I(f)+j2Z_Q(f)e^{-j2\pi f\Delta T}$. This, in turn, fits directly to the general imbalance model (2–12) for which $A_I(f)=2$ and $A_Q(f)=2e^{-j2\pi f\Delta T}$. Based on (2–13), $Z'(f)$ can then be expressed as

$$\begin{aligned} Z'(f)&=(1+e^{-j2\pi f\Delta T})Z(f)+(1-e^{-j2\pi f\Delta T})Z^*(-f)\\ &=G_{1,\mathrm{S}}(f)Z(f)+G_{2,\mathrm{S}}(f)Z^*(-f) \end{aligned} \tag{6–4}$$

where $G_{1,\mathrm{S}}(f) = (1 + e^{-j2\pi f\Delta T})$ and $G_{2,\mathrm{S}}(f) = (1 - e^{-j2\pi f\Delta T})$. Notice that these imbalance functions $G_{1,\mathrm{S}}(f)$ and $G_{2,\mathrm{S}}(f)$ are Hermitian symmetric, i.e., $G_{1,\mathrm{S}}^{*}(-f) = G_{1,\mathrm{S}}(f)$ and $G_{2,\mathrm{S}}^{*}(-f) = G_{2,\mathrm{S}}(f)$. Naturally, the actual spectrum of the discrete-time signal $z'(nT_S)$ is simply the "sampled version" of $Z'(f)$, i.e., of the form $f_S \sum_m Z'(f - mf_S)$. Based on (6–4), the image attenuation of the basic second-order sampling approach is then given by

$$L_{\mathrm{S}}(f) = \frac{|G_{1,\mathrm{S}}(f)|^2}{|G_{2,\mathrm{S}}(f)|^2} = \left| \frac{1 + \cos(2\pi f\Delta T)}{\sin(2\pi f\Delta T)} \right|^2 . \tag{6–5}$$

To illustrate, let $f_C = 100\,\mathrm{MHz}$ and $B = 25\,\mathrm{MHz}$. Then, the image attenuation $L_{\mathrm{S}}(f)$ at the edge of the useful signal band ($f = \pm B/2$) is only $20.1\,\mathrm{dB}$. Clearly, this is far from being sufficient, especially in case of wideband multichannel downconversion where the power difference of the individual channel signals can be as high as $50...100\,\mathrm{dB}$, and some additional processing is needed. For this purpose, two alternative methods for enhancing the basic image attenuation of (6–5) are proposed in Sections 6.2 and 6.3.

A graphical illustration of this whole phenomenon and of the general relation of I/Q sampling and its second-order sampling based approximation is given in Figure 6–1 for a wideband multichannel input signal. Clearly, the effect of the inherent timing difference ΔT is formally similar to the effect of amplitude and phase mismatches discussed in Chapters 2-4 (actually, using the result of (6–2), the second-order sampling can simply be viewed as to introduce a frequency-dependent phase mismatch). However, the fundamental difference is that here the imbalance arises from the known principle of sampling time difference, not from any random device mismatches. This can and will be exploited in cancelling this timing mismatch in Sections 6.2 and 6.3. Furthermore, the general approach here is also different in the sense that the multichannel nature will *not* be exploited. In other words, the image attenuation is enhanced for the signal $z'(t)$ as a whole, not on a channel-by-channel basis as was done in the proposed statistical methods in Chapter 4. For simplicity, the general signal analysis of the proposed techniques will be carried out in continuous-time domain.

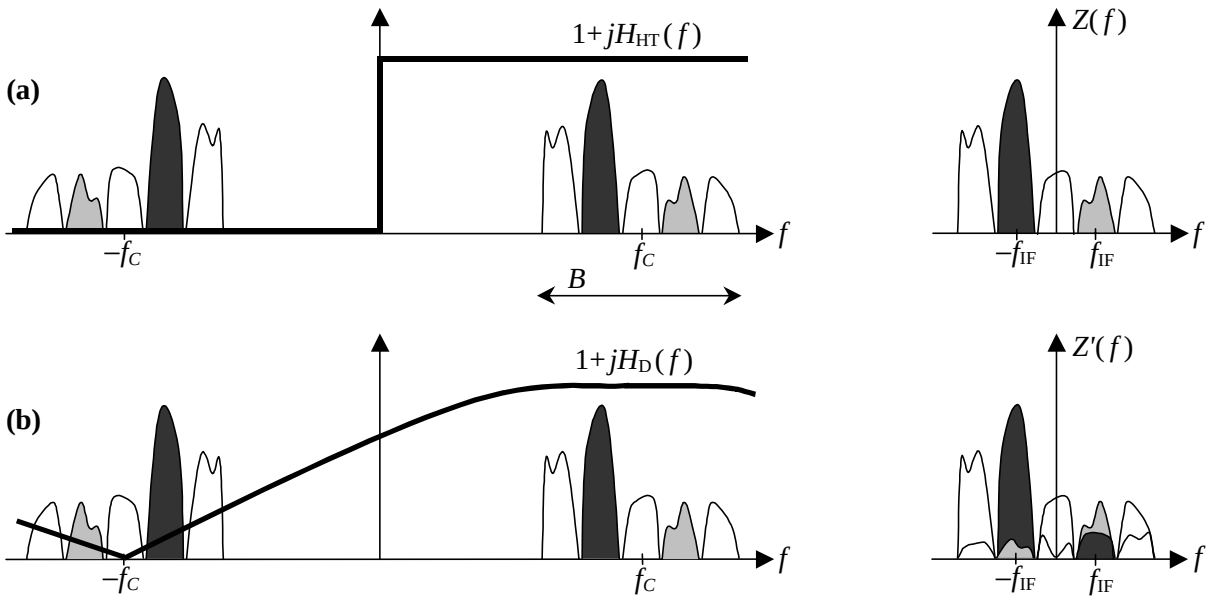

Figure 6–1: *A frequency domain illustration of the basic relation between the ideal I/Q sampling (a) and its second-order sampling based approximation (b) in case of multichannel downconversion.*

6.2 Fixed Interference Cancellation (IC)

In order to enhance the image attenuation of the basic second-order sampling scheme (i.e., to produce an accurate estimate of the baseband equivalent $z(t)$), the interference canceller type of compensation structure of Figure 6–2 is proposed. The basic idea is to use a constant coefficient (hence the name fixed) interference cancellation filter $C(f)$ together with the complex conjugate of $z'(t)$ as a reference signal to estimate and subtract the image signal interference. Let $\hat{z}(t)$ denote the compensator output signal (i.e., the estimate of $z(t)$). Then, based on the above strategy, the Fourier transform of $\hat{z}(t)$ is $\hat{Z}(f) = Z'(f) - C(f)Z'^{*}(-f)$. Using (6–4), this can be written as $\hat{Z}(f) = G_{1,\mathrm{S}}^{\mathrm{IC}}(f)Z(f) + G_{2,\mathrm{S}}^{\mathrm{IC}}(f)Z^{*}(-f)$ where

$$\begin{aligned} G_{1,\mathrm{S}}^{\mathrm{IC}}(f) &= G_{1,\mathrm{S}}(f) - C(f)G_{2,\mathrm{S}}^{*}(-f) \\ &= 1 + e^{-j2\pi f\Delta T} - C(f)(1 - e^{-j2\pi f\Delta T}) \\ G_{2,\mathrm{S}}^{\mathrm{IC}}(f) &= G_{2,\mathrm{S}}(f) - C(f)G_{1,\mathrm{S}}^{*}(-f) \\ &= 1 - e^{-j2\pi f\Delta T} - C(f)(1 + e^{-j2\pi f\Delta T}). \end{aligned} \tag{6–6}$$

As a result, the image attenuation *after* the compensation can be defined as

$$L_{\mathrm{S}}^{\mathrm{IC}}(f) = \frac{|G_{1,\mathrm{S}}^{\mathrm{IC}}(f)|^2}{|G_{2,\mathrm{S}}^{\mathrm{IC}}(f)|^2}. \tag{6–7}$$

Then, to force the image interference to zero, the compensation filter $C(f)$ is simply selected to make $G_{2,S}^{IC}(f)=0$. Clearly, this "zero forcing" solution is given by

$$C_{OPT}(f)=\frac{1-e^{-j2\pi f\Delta T}}{1+e^{-j2\pi f\Delta T}}=\frac{j\sin(2\pi f\Delta T)}{1+\cos(2\pi f\Delta T)}. \qquad (6\text{–}8)$$

Using the optimum solution of (6–8), with a reasonable bandwidth-to-center-frequency ratio (B/f_C), the gain $G_{1,S}^{IC}(f)$ of the desired component will describe a practically constant amplitude, linear phase frequency response. In other words, the effect of the image interference can be efficiently compensated without causing any notable distortion to the desired component. Also, as shown in [P6], the IC based compensation technique does not suffer from noise enhancement. Thus, $\hat{z}(t)$ will indeed be an accurate reproduction of $z(t)$ (up to a delay and multiplication by a constant). The complete enhanced second-order sampling scheme using digital interference cancellation is depicted in Figure 6–2.

In the actual digital implementation, the optimum frequency response of (6–8) can be accurately *approximated* using a real-valued impulse response with odd symmetry. Therefore, no "cross-filtering" between the real and imaginary parts of $z'(nT_S)$ is actually needed, which simplifies the implementation. One possible approach is to use a type III FIR compensation filter [64] whose impulse response c_n is odd-symmetric, i.e., $c_{-n}=-c_n$, and the frequency response is of the form

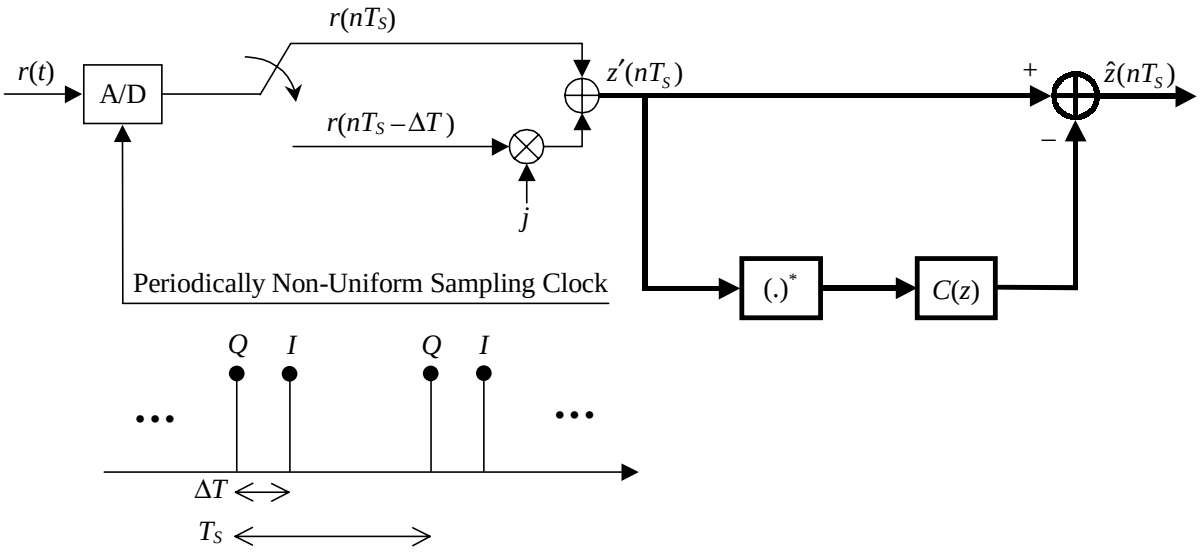

Figure 6–2: *Enhanced second-order sampling scheme based on fixed interference cancellation. Through periodically non-uniform sampling, only one actual A/D converter is needed.*

$$C(e^{j\omega}) = \sum_{k=-N}^{N} c_k e^{-j\omega k} = -2j\sum_{k=1}^{N} c_k \sin(\omega k) \tag{6–9}$$

where $2N+1$ is the filter length. In practice, due to the anti-causal nature of (6–9), the filter c_n needs to be delayed by N samples to be causal and realizable. As a consequence, the same delay needs to be introduced also in the upper branch of the IC structure.

To illustrate the performance of the proposed approach, some filter optimization results will be presented next for $N = 3$ and $N = 4$. As an example case, we study the situation for which $B = 25\,\text{MHz}$ and $f_C = 100\,\text{MHz}$. To make the filter optimization more feasible, sampling frequencies of $f_S = 50\,\text{MHz}$ and $f_S = 100\,\text{MHz}$ are used instead of the minimum usable frequency $f_S = 25\,\text{MHz}$. In this manner (due to oversampling), the optimization range $-\pi B/f_S \le \omega \le \pi B/f_S$ is only $-\pi/2 \le \omega \le \pi/2$ for $f_S = 50\,\text{MHz}$ and $-\pi/4 \le \omega \le \pi/4$ for $f_S = 100\,\text{MHz}$, respectively. In optimizing the compensation filter coefficients, both the least-squares (LS) and minimax design techniques [76] are demonstrated. The obtained results are presented in Table 6–1 in terms of the minimum obtainable image attenuation L_{S}^{IC} and the maximum of $E_{\text{IC}} = |C - C_{\text{OPT}}|$, the frequency domain approximation error function. A more detailed graphical illustration of the image attenuations is given in Figure 6–3 for $N = 4$ and $f_S = 50\,\text{MHz}$. Clearly, the obtainable image attenuation is improved significantly using the proposed approach.

6.3 Fractional Delay (FD) Filtering

An alternative and also more intuitive method to improve the basic second-order sampling scheme and its image attenuation is directly motivated by the basic signal model of (5–4). If the I branch signal $r(nT_S) = 2z_I(nT_S)$ is delayed properly relative to the Q branch signal $r(nT_S - \Delta T) = 2z_Q(nT_S - \Delta T)$, a perfect reconstruction of $z(nT_S)$ will follow (again, up to a delay and multiplication by a constant). However, using a sampling frequency $f_S = f_C/r$, the needed delay $\Delta T = 1/(4f_C) = T_S/(4r)$ is only a fraction of the sampling interval. Therefore, a digital fractional delay filter (see, e.g., [51] and [87]) is a convenient choice to implement this function. The basic block diagram of the enhanced second-order sampling scheme exploiting this idea is presented in Figure 6–4.

Again, for notational convenience, the signal analysis of the proposed scheme is carried out in continous-time domain. First, denoting the frequency response of the fractional delay filter by $D(f)$, the compensated output signal $\hat{z}(t)$ can be expressed in frequency domain as $\hat{Z}(f) = 2Z_I(f)D(f) + j2Z_Q(f)e^{-j2\pi f\Delta T}$. Based on the general imbalance model (2–13), this can be written also as $\hat{Z}(f) = G_{1,\text{S}}^{\text{FD}}(f)Z(f) + G_{2,\text{S}}^{\text{FD}}(f)Z^*(-f)$ where

Table 6–1: *IC filter optimization results. Filter length is* $2N + 1$.

	B / f_S	$\min(L_S^{IC})$ [dB]		$\max(E_{IC})$	
		LS	MINIMAX	LS	MINIMAX
$N = 3$	1/2	65.1	72.2	5.6×10^{-4}	2.4×10^{-4}
	1/4	103.3	110.6	6.9×10^{-6}	3.0×10^{-6}
$N = 4$	1/2	80.4	88.6	9.6×10^{-5}	3.7×10^{-5}
	1/4	131.5	139.7	2.7×10^{-7}	1.0×10^{-7}

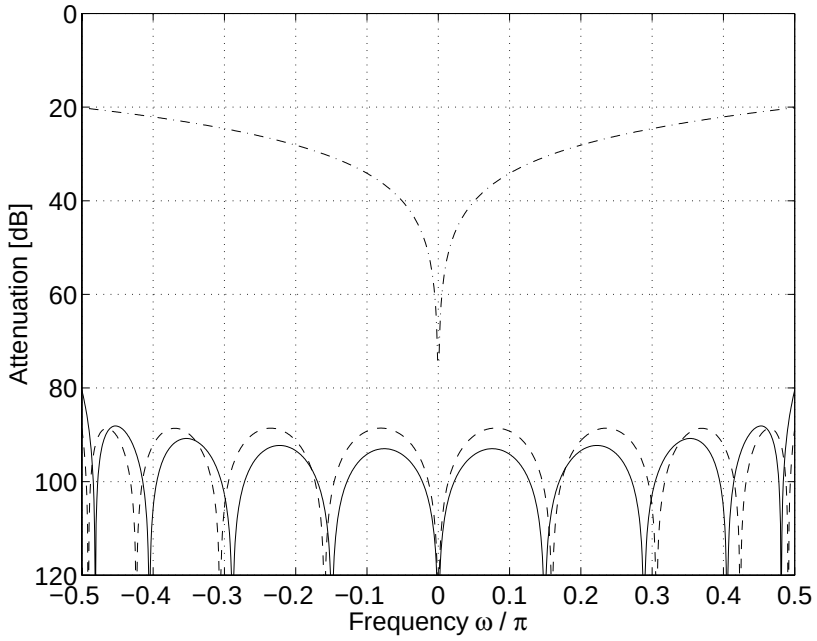

Figure 6–3: *Image signal attenuations of the IC based enhanced second-order sampling scheme for LS (solid) and minimax (dashed) optimized compensation filters for* $N = 4$ *and* $f_S = 50$ *MHz. Also shown is the image attenuation of the basic second-order sampling technique (dash-dotted).*

$$G_{1,S}^{FD}(f) = D(f) + e^{-j2\pi f\Delta T}$$
$$G_{2,S}^{FD}(f) = D(f) - e^{-j2\pi f\Delta T}. \tag{6–10}$$

Then, analogously to (6–5) and (6–7), the image attenuation of the fractional delay filtering based technique can be defined as

$$L_S^{FD}(f) = \frac{|G_{1,S}^{FD}(f)|^2}{|G_{2,S}^{FD}(f)|^2}. \tag{6–11}$$

Naturally, based on (6–10), the ideal delay response $D(f) = e^{-j2\pi f\Delta T}$ results in complete elimination of the image as $\hat{z}(t) = 2z(t - \Delta T)$.

Considering the digital implementation, let $d = \Delta T / T_S = 1/(4r)$ denote the normalized fractional delay. Then, the frequency response of the ideal digital FD filter is given by

$$D_{\mathrm{OPT}}(e^{j\omega}) = e^{-j\omega d}. \tag{6–12}$$

In practice, using a finite order FIR or infinite impulse response (IIR) filter, this response can only be approximated. One possibility to do the approximation is to use an FIR filter of length $2N$ whose frequency response is in general of the form

$$D(e^{j\omega}) = \sum_{k=-N+1}^{N} d_k e^{-j\omega k}. \tag{6–13}$$

Again, in a practical implementation, the filter needs to be delayed by $N-1$ samples to make it realizable and the Q branch signals needs to be delayed accordingly.

For comparison, we study exactly the same example situation ($B = 25\,\mathrm{MHz}$ and $f_C = 100\,\mathrm{MHz}$) as in Section 6.2. In the approximation, FIR filters of (6–13) are used with $N = 3$ and $N = 4$. The results of both the least-squares and minimax optimization are given in Table 6–2, showing again the minimum obtainable image attenuation and the maximum of the error function $E_{\mathrm{FD}} = |D - D_{\mathrm{OPT}}|$. A more detailed illustration of the image attenuation behaviour is given in Figure 6–5.

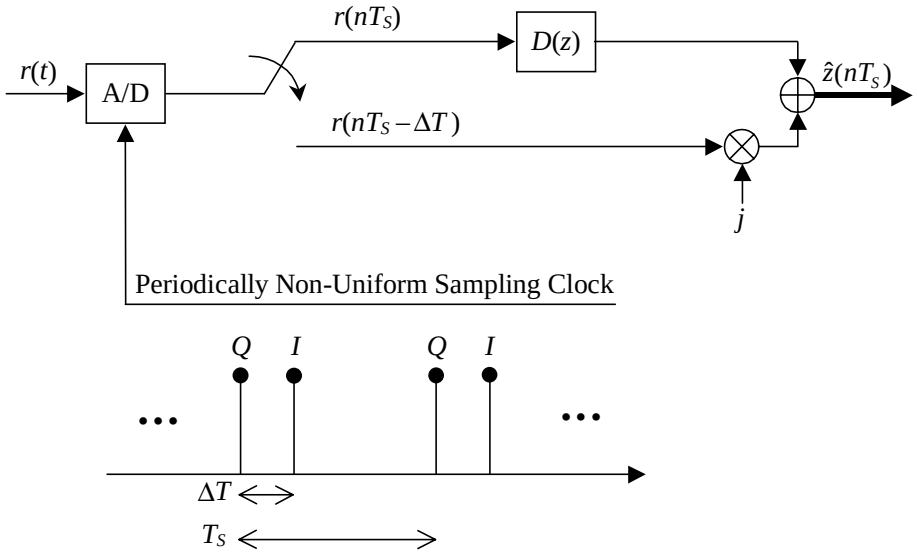

Figure 6–4: *Enhanced second-order sampling scheme based on fractional delay filtering. Through periodically non-uniform sampling, only one actual A/D converter is needed.*

Table 6–2: *FD filter optimization results. Filter length is* $2N$.

	B / f_S	d	$\min(L_S^{FD})$ [dB]		$\max(E_{FD})$	
			LS	MINIMAX	LS	MINIMAX
$N = 3$	1/2	1/8	57.2	63.9	2.7×10^{-3}	1.3×10^{-3}
	1/4	1/4	90.2	96.8	6.2×10^{-5}	2.9×10^{-5}
$N = 4$	1/2	1/8	72.6	80.4	4.7×10^{-4}	1.9×10^{-4}
	1/4	1/4	118.3	125.8	2.4×10^{-6}	1.0×10^{-6}

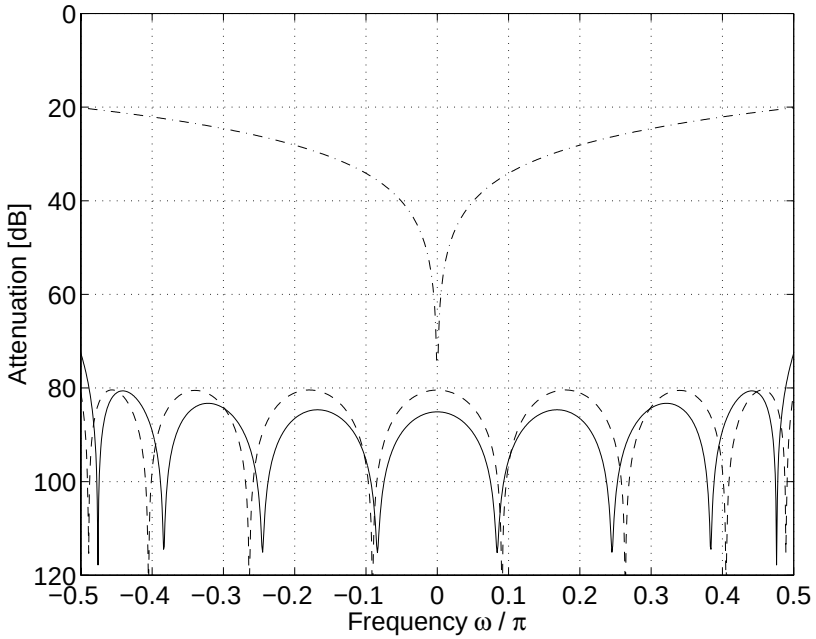

Figure 6–5: *Image signal attenuations of the FD filter based enhanced second-order sampling scheme for LS (solid) and minimax (dashed) optimized compensation filters for* $N = 4$ *and* $f_S = 50$ *MHz. Also shown is the image attenuation of the basic second-order sampling technique (dash-dotted).*

6.4 Comparisons and Practical Considerations

Two alternative methods to enhance the image attenuation of the basic second-order sampling scheme were proposed. Though these two approaches are based on totally different ideas, they both provide powerful solutions in compensating the inherent timing difference and thus enhancing the demodulation quality. Using compensation filters of length $2N+1$ (IC) and $2N$ (FD), respectively, both techniques need only $2N$ real multiplications per complex-valued output sample. On one hand, with fixed number of arithmetic operations, the IC technique provides slightly higher image attenuation. This is clearly evidenced by the

presented optimization results. On the other hand, the FD filtering based method is more flexible in the sense that the delay parameter d can be easily controlled. This can be achieved, e.g., by using the polynomial based interpolation techniques [51], [87]. In general, using either of the proposed approaches, image attenuations in the order of $80...120\,\text{dB}$ are theoretically achievable, even with very short compensation filters ($N = 3...5$). It should be noted, however, that any unintentional error or jitter[11] in the sampling instants can and will degrade the system performance. Therefore, as in any other high performance sampled data system, an accurate and stable reference clock is needed.

From the radio systems point of view, the previous subsampling based demodulation techniques constitute some demands for the A/D conversion process and also for the system and receiver parameters. First of all, the wideband sampling approach sets high demands for the A/D converter dynamic range. Also, the general concept of bandpass sampling sets tight requirements for the A/D converter speed and the sampling clock jitter. In effect, any deviations from the ideal sampling instants result in additional phase mismatch, compromising again the image attenuation. Also, due to noise aliasing, the subsampling ratio f_C / f_S should be kept at a reasonably low level. As a result, the proposed approaches are limited with the state of the art components mainly to center-frequencies of around $100...200\,\text{MHz}$ and to sampling frequencies of a few tens of MHz. In other words, in wireless communications applications, an initial wideband downconversion from the GHz range to a lower intermediate frequency is needed. All the previous problems are, however, common to any digital signal processing based solution and are expected to be relieved with constantly improving circuit technologies.

[11] Any short-term variation or instability of the significant instances of a digital data or clock signal with respect to their ideal positions in time is generally termed jitter.

Chapter 7

Conclusions

The current trend in wireless transceiver design is to simplify the analog front-end processing as much as possible and implement most of the fundamental functions using digital signal processing. This is mainly motivated by the ever-increasing flexibility and integrability requirements to access multiple wireless standards and services using a single, small-size, small-cost user equipment. As a consequence, the traditional superheterodyne architecture is not the most appropriate choice and new receiver structures, such as the low-IF receiver, are under active investigation.

One of the most fundamental tasks of any radio receiver is to downconvert the desired channel signal from RF range closer to baseband. In this context, the inherent image signal problem needs to be addressed with care. One interesting approach relaxing the requirements for RF filtering is to use I/Q downconversion. This approach, like any other application of analog I/Q processing, is susceptible to branch mismatches. These mismatches indeed compromise the theoretically infinite image attenuation to only 20-40 dB range in practical analog implementations.

In this thesis, various I/Q signal processing techniques in communications receivers were discussed and analyzed. As the main contribution, digital I/Q imbalance compensation was addressed in detail. Two alternative techniques based on interference cancellation and blind signal separation were proposed to enhance the analog front-end image attenuation. These compensation strategies were motivated by the presented baseband signal model consisting of two signals: a desired signal observation and an interference observation. The theoretical compensation performance of the proposed methods was assessed analytically and shown to be sufficient for practical communications applications. In general, the imbalance compensation can be performed blindly since no training signals are needed. Due to their inherent adaptive nature, the proposed methods are also capable of tracking possible time-

variations in the front-end imbalances. Furthermore, the challenging case of frequency-dependent imbalances can be handled as well.

One basic assumption in the derivations of the proposed compensators was that the imbalance effects can be modelled as a linear system. In practical implementations, however, the non-linear effects of the analog circuitry cannot be avoided. Probably this, together with the receiver noise figure (NF) and finite word-length of digital processing as well as the limited dynamic range of A/D converters, will turn out to reduce the performance of the proposed compensation methods, especially in case of strong interfering signals. This calls for proper modelling of these non-idealities and/or co-simulation of the analog and digital parts to get the right picture of the performance of the proposed approaches. This constitutes one important topic for further work and research. In addition, blind signal separation techniques for non-linear mixture models (see, e.g., [43]) could form an interesting topic for further studies as well.

Motivated by the continuously advancing A/D conversion technologies, second-order sampling based quadrature demodulation was also considered. After a detailed image attenuation analysis, two digital schemes utilizing fixed interference cancellation or fractional delay filtering were proposed to enhance the demodulation performance. As illustrated by the analysis and design examples, the proposed techniques result in a significant improvement in attenuating the image band signal.

All bandpass sampling based digital downconversion techniques, such as the second-order sampling based one considered in this thesis, constitute strict requirements for the A/D conversion process. A high speed, high dynamic range converter is in general needed with an accurate sampling clock. One good topic for further studies could be to model these practical phenomena in a proper manner in order to analyze their effect on the system performance. Especially, characterizing the non-idealities of a non-uniform clock signal in the second-order sampling scheme is an interesting topic for future work.

Chapter 8

Summary of Publications

The fundamental idea of viewing the I/Q imbalance compensation task as a signal enhancement problem is originally introduced in [P1]. The basic frequency-independent signal model consisting of two baseband observations is also proposed in [P1] together with the adaptive interference canceller based compensation strategy. In [P2], a thorough performance analysis of the IC based compensator is presented. The natural performance index is the steady-state SIR at the compensator output signal. As shown by the analysis, an adaptive interference canceller using, e.g., the LMS algorithm can provide sufficient compensation performance. This analysis gives a formal validation for the whole IC based compensation method. In addition to IC processing, an alternative compensation strategy is proposed in [P3]. There, the idea is to undo the image interference using blind signal separation techniques. Though also of general importance, these techniques can be viewed here as a generalization of traditional interference cancellation where also the signal leakage phenomenon is addressed in a novel manner. Motivated by exactly the same signal model, a unified treatment of both the IC and BSS based compensation techniques is given in [P4]. Though the main emphasis in the presentation is on the signal processing aspects, also the effects of additive noise, symbol timing errors, and especially the type of the desired and interfering signals are discussed in a comparative manner. This paper can be clearly regarded as the core of this thesis. While [P1] - [P4] mainly concentrates on the frequency-independent imbalance model, the effects of frequency-selective mismatches are addressed in [P5]. There, a general frequency domain signal model is presented for an imbalanced analog front-end processing, and the previously proposed compensation strategies are extended to handle this kind of frequency-dependent imbalances as well.

Papers [P6] and [P7] consider the second-order sampling based quadrature demodulation. In [P6], a detailed analysis is given for the basic second-order sampling

scheme and its connection to the ideal I/Q sampling is discussed. Furthermore, the idea of using fixed interference cancellation to improve the image signal attenuation is proposed and analyzed. Also, some compensation filter design examples are given together with an illustrative example simulation. In [P7], fractional delay filtering based processing is proposed as an alternative to interference cancellation to enhance the demodulation quality. Its performance is analyzed and a practical example design is given.

8.1 Author's Contribution to the Publications

The research work for this thesis was carried out at the Telecommunications Laboratory, Tampere University of Technology as an individual part of larger research projects "Analog and Digital Signal Processing Techniques for Highly Integrated Transceivers" and "Advanced Transceiver Architectures and Implementations for Wireless Communications". In general, all the I/Q signal processing research reported in this thesis was done by the Author alone yet naturally supported and guided by the thesis supervisors Prof. Renfors and Prof. Koivunen. Thus, the Author is the primary author in all the original papers [P1] - [P7]. It goes without saying that the numerous informal discussions between the Author and the supervisors have contributed to the reported results as well as to the general research directions considerably.

Originally, Prof. Renfors introduced the I/Q imbalance problem to the Author. Furthermore, the credit for initially viewing the imbalance problem in frequency domain and especially utilizing the inherent frequency diversity belongs to the thesis supervisors Prof. Renfors and Prof. Koivunen. Since then, the Author has developed all the signal models, carried out all the performance analyses, and performed the computer simulations reported in the original papers [P1] - [P5]. In addition, all the writing was done by the Author. Naturally, the coauthors Prof. Renfors and Prof. Koivunen contributed to the final appearance of each paper.

The second-order sampling based quadrature demodulation scheme and it's relation to the imbalance problem was originally introduced to the Author by Prof. Renfors. The compensation strategies proposed in [P6] and [P7] were then developed and analyzed by the Author who also did the writing and preparation of those papers.

Bibliography

[1] A. A. Abidi, “Direct conversion radio transceivers for digital communications,” *IEEE J. Solid-State Circuits*, vol. 30, pp. 1399-1410, Dec. 1995.

[2] A. A. Abidi, “CMOS wireless transceiver: The new wave,” *IEEE Commun. Mag.*, vol. 37, pp. 119-124, Aug. 1999.

[3] A. A. Abidi, “Low-power radio-frequency ICs for portable communications,” in L. E. Larson, Ed., *RF and Microwave Circuit Design for Wireless Communications*. Norwood, MA: Artech House, 1996, pp. 43-98.

[4] S. Amari, S. C. Douglas, A. Cichocki, and H. H. Yang, “Multi-channel blind deconvolution and equalization using the natural gradient,” *in Proc. IEEE Workshop Signal Processing Adv. Wireless Commun.*, Paris, France, Apr. 1997, pp. 101-104.

[5] E. Buracchini, “The software radio concept,” *IEEE Commun. Mag.*, vol. 38, pp. 138-143, Sept. 2000.

[6] J.-F. Cardoso, “Blind source separation: Statistical principles,” *Proc. IEEE*, vol. 86, pp. 2009-2025, Oct. 1998.

[7] J.-F. Cardoso and B. H. Laheld, “Equivariant adaptive source separation,” *IEEE Trans. Signal Processing*, vol. 44, pp. 3017-3030, Dec. 1996.

[8] A. B. Carlson, *Communication Systems*, 3rd ed. New York: McGraw-Hill, 1986.

[9] J. K. Cavers and M. W. Liao, “Adaptive compensation for imbalance and offset losses in direct conversion transceivers,” *IEEE Trans. Veh. Technol.*, vol. 42, pp. 581-588, Nov. 1993.

[10] E. Cetin, I. Kale, and R. C. S. Morling, “Adaptive compensation of analog front-end I/Q mismatches in digital receivers,” in *Proc. IEEE Int. Symp. Circuits Syst.*, Sydney, Australia, May 2001, pp. 370-373.

[11] J. Y. C. Cheah, “Introduction to wireless communications applications and circuit design,” in L. E. Larson, Ed., *RF and Microwave Circuit Design for Wireless Communications*. Norwood, MA: Artech House, 1996, pp. 17-41.

[12] C. Chien, *Digital Radio Systems on a Chip – A Systems Approach*. Norwell, MA: Kluwer Academic Publishers, 2001.

[13] S. Choi, A. Cichocki, and S. Amari, "Flexible independent component analysis," in *Proc. IEEE Signal Processing Soc. Workshop Neural Networks Signal Processing*, Cambridge, UK, Aug. 1998, pp. 83-92.

[14] L. W. Couch, *Digital and Analog Communication Systems*, 6th ed. Upper Saddle River, NJ: Prentice-Hall, 2001.

[15] A. J. Coulson, "A generalization of nonuniform bandpass sampling," *IEEE Trans. Signal Processing*, vol. 43, pp. 694-704, Mar. 1995.

[16] A. J. Coulson, R. G. Vaughan, and M. A. Poletti, "Frequency-shifting using bandpass sampling," *IEEE Trans. Signal Processing*, vol. 42, pp. 1556-1559, June 1994.

[17] J. Crols and M. S. J. Steyaert, "An analog integrated polyphase filter for a high performance low-IF receiver," in *IEEE Symp. VLSI Circuits Dig. Tech. Papers*, Kyoto, Japan, June 1995, pp. 87-88.

[18] J. Crols and M. S. J. Steyaert, "A 1.5 GHz highly linear CMOS downconversion mixer," *IEEE J. Solid-State Circuits*, vol. 30, pp. 736-742, July 1995.

[19] J. Crols and M. S. J. Steyaert, "A single-chip 900 MHz CMOS receiver front-end with a high performance low-IF topology," *IEEE J. Solid-State Circuits*, vol. 30, pp. 1483-1492, Dec. 1995.

[20] J. Crols and M. S. J. Steyaert, "Low-IF topologies for high-performance analog front ends of fully integrated receivers," *IEEE Trans. Circuits Syst. II*, vol. 45, pp. 269-282, Mar. 1998.

[21] J. Crols and M. S. J. Steyaert, *CMOS Wireless Transceiver Design*. Dordrecht, the Netherlands: Kluwer Academic Publishers, 1997.

[22] V. Eerola, T. Ritoniemi, and H. Tenhunen, "Second-order sampling and oversampled A/D- and D/A-converters in digital data transmission," in *Proc. IEEE Int. Symp. Circuits Syst.*, Singapore, June 1991, pp. 1521-1524.

[23] R. H. Engelmann, "The origins of radio," *IEEE Potentials*, vol. 19, pp. 41-44, Oct.-Nov. 2000.

[24] M. Faulkner, T. Mattsson, and W. Yates, "Automatic adjustment of quadrature modulators," *Electron. Lett.*, vol. 27, pp. 214-216, Jan. 1991.

[25] W. Feixue, Y. Shaowei, and G. Guirong, "Mixer-free digital quadrature demodulation based on second-order sampling," *Electron. Lett.*, vol. 34, pp. 854-855, Apr. 1998.

[26] L. E. Franks, *Signal Theory*. Englewood Cliffs, NJ: Prentice-Hall, 1969.

[27] M. E. Frerking, *Digital Signal Processing in Communication Systems*. New York: Chapman & Hall, 1994.

[28] A. Gatherer, T. Stetzler, M. McMahan, and E. Auslander, "DSP-based architectures for mobile communications: Past, present and future," *IEEE Commun. Mag.*, vol. 38, pp. 84-90, Jan. 2000.

[29] J. P. F. Glas, "Digital I/Q imbalance compensation in a low-IF receiver," in *Proc. IEEE Global Telecommun. Conf.*, Sydney, Australia, Nov. 1998, pp. 1461-1466.

[30] R. A. Green, "An optimized multi-tone calibration signal for quadrature receiver communication systems," in *Proc. IEEE Workshop Statist. Signal Array Processing*, Pocono Manor, PA, USA, Aug. 2000, pp. 664-667.

[31] R. A. Green, R. Anderson-Sprecher, and J. W. Pierre, "Quadrature receiver mismatch calibration," *IEEE Trans. Signal Processing*, vol. 47, pp. 3130-3133, Nov. 1999.

[32] J. E. Gunn, K. S. Barron, and W. Ruczczyk, "A low-power DSP core-based software radio architecture," *IEEE J. Select. Areas Commun.*, vol. 17, pp. 574-590, Apr. 1999.

[33] S. L. Hahn, *Hilbert Transforms in Signal Processing*. Norwood, MA: Artech House, 1996.

[34] L. Hanzo, "Bandwidth-efficient wireless multimedia communications," *Proc. IEEE*, vol. 86, pp. 1342-1382, July 1998.

[35] f. harris, "Digital filter equalization of analog gain and phase mismatch in I-Q receivers," in *Proc. IEEE Int. Conf. Univ. Pers. Commun.*, Cambridge, MA, USA, Sept. 1996, pp. 793-796.

[36] S. Haykin, *Adaptive Filter Theory*, 3rd ed. Upper Saddle River, NJ: Prentice-Hall, 1996.

[37] S. Haykin, Ed., *Unsupervised Adaptive Filtering, vol I: Blind Source Separation*. New York: John Wiley & Sons, 2000.

[38] S. Haykin, *Communication Systems*, 4th ed. New York: John Wiley & Sons, 2001.

[39] T. Hentschel and G. Fettweis, "Software radio receivers," in F. Swarts, P. van Rooyan, I. Oppermann, and M. P. Lötter, Eds., *CDMA Techniques for Third Generation Mobile Systems*. Norwell, MA: Kluwer Academic Publishers, 1999, pp. 257-283.

[40] T. Hentschel, M. Henker, and G. Fettweis, "The digital front-end of software radio terminals," *IEEE Pers. Commun.*, vol. 6, pp. 40-46, Aug. 1999.

[41] D. Hilborn, S. P. Stapleton, and J. K. Cavers, "An adaptive direct conversion transmitter," *in Proc. IEEE Veh. Technol. Conf.*, Denver, CO, USA, June 1992, pp. 764-767.

[42] A. Hyvärinen, "A family of fixed-point algorithms for independent component analysis," in *Proc. IEEE Int. Conf. Acoust., Speech, Signal Processing*, Munich, Germany, Apr. 1997, pp. 3917-3920.

[43] A. Hyvärinen, J. Karhunen, and E. Oja, *Independent Component Analysis*. New York: John Wiley & Sons, 2001.

[44] S. A. Jantzi, K. W. Martin, and A. S. Sedra, "Quadrature bandpass delta-sigma modulation for digital radio," *IEEE J. Solid-State Circuits*, vol. 32, pp. 1935-1950, Dec. 1997.

[45] Y.-C. Jeng, "Perfect reconstruction of digital spectrum from nonuniformly sampled signals," *IEEE Trans. Instrum. Meas.*, vol. 46, pp. 649-652, June 1997.

[46] H. Jin and E. K. F. Lee, "A digital-background calibration technique for minimizing timing-error effects in time-interleaved ADC's," *IEEE Trans. Circuits Syst. II*, vol. 47, pp. 603-613, July 2000.

[47] J. Karhunen, E. Oja, L. Wang, R. Vigário, and J. Joutsensalo, "A class of neural networks for independent component analysis," *IEEE Trans. Neural Networks*, vol. 8, pp. 486-504, May 1997.

[48] H. R. Karimi and B. Friedrichs, "Wideband digital receivers for multi-standard software radios," in *IEE Coll. Adaptable Multi-Standard Mobile Radio Terminals*, London, UK, Mar. 1998, pp. 5/1-5/7.

[49] T. E. Kolding, "Multi-standard mixed-signal transceivers for wireless communications – A research overview," Department of Communication Technology, Aalborg University, Aalborg, Denmark, Tech. Rep. R-96-1005, Dec. 1996.

[50] M. Kozak and I. Kale, "Novel topologies for time-interleaved delta-sigma modulators," *IEEE Trans. Circuits Syst. II*, vol. 47, pp. 639-654, July 2000.

[51] T. I. Laakso, V. Välimäki, M. Karjalainen, and U. K. Laine, "Splitting the unit delay," *IEEE Signal Processing Mag*., vol. 13, pp. 30-60, Jan. 1996.

[52] E. A. Lee and D. G. Messerschmitt, *Digital Communication*. Boston, MA: Kluwer Academic Publishers, 1988.

[53] J. P. Y. Lee, "Wideband I/Q demodulators: Measurement technique and matching characteristics," *IEE Proc. Radar, Sonar, Navigation*, vol. 143, pp. 300-306, Oct. 1996.

[54] Y.-P. Lin and P. P. Vaidyanathan, "Periodically nonuniform sampling of bandpass signals," *IEEE Trans. Circuits Syst. II*, vol. 45, pp. 340-351, Mar. 1998.

[55] A. Lohtia, P. A. Gould, and C. G. Englefield, "An adaptive digital technique for compensating for analog quadrature modulator / demodulator impairments," *in Proc. IEEE Pacific Rim Conf. Commun., Comput., Signal Processing*, Victoria, BC, Canada, May 1993, pp. 447-450.

[56] W. W. Lu, "Compact multidimensional broadband wireless: The convergence of wireless mobile and access," *IEEE Commun. Mag.*, vol. 38, pp. 119-123, Nov. 2000.

[57] J. M. Mendel, *Lessons in Estimation Theory for Signal Processing, Communications and Control*. Englewood Cliffs, NJ: Prentice-Hall, 1995.

[58] H. Meyr, M. Moeneclay, and S. A. Fechtel, *Digital Communication Receivers*. New York: John Wiley & Sons, 1998.

[59] S. Mirabbasi and K. Martin, "Classical and modern receiver architectures," *IEEE Commun. Mag.*, vol. 38, pp. 132-139, Nov. 2000.

[60] R. L. Mitchell, "Creating complex signal samples from a band-limited real signal," *IEEE Trans. Aerosp. Electron. Syst.*, vol. 25, pp. 425-427, May 1989.

[61] J. Mitola, *Software Radio Architecture: Object-Oriented Approaches to Wireless Systems Engineering*. New York: John Wiley & Sons, 2000.

[62] H. Nguyen, "Improving QPSK demodulator performance for quadrature receiver with information from amplitude and phase imbalance correction," *in Proc. IEEE Wireless Commun. Networking Conf.*, Chicago, IL, USA, Sept. 2000, pp. 1440-1444.

[63] T. Okanobu, H. Tomiyama, and H. Arimoto, "Advanced low voltage single chip radio IC," *IEEE Trans. Consumer Electron.*, vol. 38, pp. 465-475, Aug. 1992.

[64] A. V. Oppenheim and R. W. Schafer, *Discrete-Time Signal Processing*. Englewood Cliffs, NJ: Prentice-Hall, 1989.

[65] J. M. Paez-Borrallo and F. J. Casajus Quiros, "Self adjusting digital image rejection receiver for mobile communications," *in Proc. IEEE Veh. Technol. Conf.*, Phoenix, AZ, USA, May 1997, pp. 686-690.

[66] J. W. Pierre and D. R. Fuhrmann, "Considerations in the autocalibration of quadrature receivers," in *Proc. IEEE Int. Conf. Acoust., Speech, Signal Processing*, Detroit, MI, USA, May 1995, pp. 1900-1903.

[67] J. G. Proakis, *Digital Communications*, 3rd ed. New York: McGraw-Hill, 1995.

[68] K.-P. Pun, J. E. Franca, and C. Azeredo-Leme, "Wideband digital correction of I and Q mismatch in quadrature radio receivers," in *Proc. IEEE Int. Symp. Circuits Syst.*, Geneva, Switzerland, May 2000, pp. 661-664.

[69] C. M. Rader, "A simple method for sampling in-phase and quadrature components," *IEEE Trans. Aerosp. Electron. Syst.*, vol. 20, pp. 821-824, Nov. 1984.

[70] T. S. Rappaport, *Wireless Communications: Principles and Practice*. Upper Saddle River, NJ: Prentice-Hall, 1996.

[71] B. Razavi, "Design considerations for direct-conversion receivers," *IEEE Trans. Circuits Syst. II*, vol. 44, pp. 428-435, June 1997.

[72] B. Razavi, "RF IC design challenges," in *Proc. Design Autom. Conf.*, San Francisco, CA, USA, June 1998, pp. 408-413.

[73] U. L. Rohde, J. Whitaker, and T. T. N. Bucher, *Communications Receivers: Principles and Design*, 2nd ed. New York: McGraw-Hill, 1997.

[74] S. J. Roome, "Analysis of quadrature detectors using complex envelope notation," *IEE Proc. Radar and Signal Processing*, vol. 136, pp. 95-100, Apr. 1989.

[75] J. C. Rudell *et al*., "A 1.9-GHz wide-band IF double conversion CMOS receiver for cordless telephone applications," *IEEE J. Solid-State Circuits*, vol. 32, pp. 2071-2088, Dec. 1997.

[76] T. Saramäki, "Finite impulse response filter design," in S. K. Mitra and J. F. Kaiser, Eds., *Handbook for Digital Signal Processing*. New York: John Wiley & Sons, 1993, pp. 155-277.

[77] J. Sevenhans, B. Verstraeten, and S. Taraborrelli, "Trends in silicon radio large scale integration: Zero IF receiver! Zero I&Q transmitter! Zero discrete passives!," *IEEE Commun. Mag.*, vol. 38, pp. 142-147, Jan. 2000.

[78] D. K. Shaeffer and T. H. Lee, *The Design and Implementation of Low-Power CMOS Radio Receivers*. Boston, MA: Kluwer Academic Publishers, 1999.

[79] E. Song, S.-I. Chae, and W. Kim, "A 2 GHz CMOS double conversion downconverter with robust image rejection performance against the process and temperature variations," in *IEEE Symp. VLSI Circuits Dig. Tech. Papers*, Honolulu, HI, USA, June 2000, pp. 38-41.

[80] M. S. J. Steyaert and R. Roovers, "A 1-GHz single-chip quadrature modulator," *IEEE J. Solid-State Circuits*, vol. 27, pp. 1194-1197, Aug. 1992.

[81] M. S. J. Steyaert *et al*., "A 2-V CMOS cellular transceiver front-end," *IEEE J. Solid-State Circuits*, vol. 35, pp. 1895-1907, Dec. 2000.

[82] J. Tsui, *Digital Techniques for Wideband Receivers*. Norwood, MA: Artech House, 1995.

[83] H. Tsurumi and Y. Suzuki, "Broadband RF stage architecture for software-defined radio in handheld terminal applications," *IEEE Commun. Mag.*, vol. 37, pp. 90-95, Feb. 1999.

[84] H. Tsurumi *et al*., "Broadband and flexible receiver architecture for software defined radio terminal using direct conversion and low-IF principle," *IEICE Trans. Commun.*, vol. E83-B, pp. 1246-1253, June 2000.

[85] M. Valkama, *Advanced DSP for I/Q Imbalance Compensation in Digital Receivers*. M.Sc. Thesis, Tampere, Finland: Tampere University of Technology, Department of Electrical Engineering, Jan. 2000.

[86] R. G. Vaughan, N. L. Scott, and D. R. White, "The theory of bandpass sampling," *IEEE Trans. Signal Processing*, vol. 39, pp. 1973-1984, Sept. 1991.

[87] J. Vesma and T. Saramäki, "Optimization and efficient implementation of fractional delay FIR filters," in *Proc. Third IEEE Int. Conf. Electronics, Circuits, Syst.*, Rhodes, Greece, Oct. 1996, pp. 546-549.

[88] E. Weinstein, M. Feder, and A. V. Oppenheim, "Multi-channel signal separation by decorrelation," *IEEE Trans. Speech Audio Processing*, vol. 1, pp. 405-413, Oct. 1993.

[89] J. A. Weppman, "Analog-to-digital converters and their applications in radio receivers," *IEEE Commun. Mag.*, vol. 33, pp. 39-45, May 1995.

[90] B. Widrow and S. D. Stearns, *Adaptive Signal Processing*. Englewood Cliffs, NJ: Prentice-Hall, 1985.

[91] S. Wu and B. Razavi, "A 900-MHz/1.8-GHz CMOS receiver for dual-band applications," *IEEE J. Solid-State Circuits*, vol. 33, pp. 2178-2185, Dec. 1998.

[92] D. T. S. Yim and C. C. Ling, "A 200-MHz CMOS I/Q downconverter," *IEEE Trans. Circuits Syst. II*, vol. 46, pp. 808-810, June 1999.

[93] L. Yu and W. M. Snelgrove, "A novel adaptive mismatch cancellation system for quadrature IF radio receivers," *IEEE Trans. Circuits Syst. II*, vol. 46, pp. 789-801, June 1999.

[94] K. C. Zangi and R. D. Koilpillai, "Software radio issues in cellular base stations," *IEEE J. Select. Areas Commun.*, vol. 17, pp. 561-573, Apr. 1999.

[95] M. Zeng, A. Annamalai, and V. K. Bhargava, "Recent advances in cellular wireless Communications," *IEEE Commun. Mag.*, vol. 37, pp. 128-138, Sept. 1999.

Publications

Publication 1

M. Valkama and M. Renfors, “Advanced DSP for I/Q imbalance compensation in a low-IF receiver,” in *Proc. IEEE International Conference on Communications*, New Orleans, LA, USA, June 2000, pp. 768-772.

Publication 2

M. Valkama, M. Renfors, and V. Koivunen, “On the performance of interference canceller based I/Q imbalance compensation,” in *Proc. IEEE International Conference on Acoustics, Speech, and Signal Processing*, Istanbul, Turkey, June 2000, pp. 2885-2888.

Publication 3

M. Valkama, M. Renfors, and V. Koivunen, “Blind source separation based I/Q imbalance compensation,” in *Proc. IEEE Symposium 2000 on Adaptive Systems for Signal Processing, Communications, and Control*, Lake Louise, AL, Canada, Oct. 2000, pp. 310-314.

Publication 4

M. Valkama, M. Renfors, and V. Koivunen, “Advanced methods for I/Q imbalance compensation in communication receivers,” *IEEE Transactions on Signal Processing*, vol. 49, pp. 2335-2344, Oct. 2001.

Publication 5

M. Valkama, M. Renfors, and V. Koivunen, “Compensation of frequency-selective I/Q imbalances in wideband receivers: Models and algorithms,” in *Proc. Third IEEE Workshop on Signal Processing Advances in Wireless Communications*, Taoyuan, Taiwan, R.O.C., Mar. 2001, pp. 42-45.

Publication 6

M. Valkama and M. Renfors, “A novel image rejection architecture for quadrature radio receivers,” submitted to *IEEE Transactions on Circuits and Systems II*.

Publication 7

M. Valkama and M. Renfors, “Second-order sampling of wideband signals,” in *Proc. IEEE International Symposium on Circuits and Systems*, Sydney, Australia, May 2001, pp. 801-804.

Tampereen teknillinen korkeakoulu
PL 527
33101 Tampere

Tampere University of Technology
P. O. B. 527
FIN-33101 Tampere Finland